GA-A12894
UC-77 Gas Cooled
Reactor Technology

GAS-COOLED FAST BREEDER REACTOR

QUARTERLY PROGRESS REPORT

FOR THE PERIOD NOVEMBER 1, 1973 THROUGH JANUARY 31, 1974

by

Project Staff

Prepared for the
U.S. Atomic Energy Commission
San Francisco Operations Office
Under
Contract AT(04-3)-167
Project Agreement No. 23

General Atomic Project 393

April 12, 1974

GENERAL ATOMIC

GENERAL ATOMIC COMPANY
P.O. BOX 81608
SAN DIEGO, CALIFORNIA 92138

PROGRESS REPORT SERIES

GA-5537	November 1, 1963 to July 31, 1964
GA-6667	August 1, 1964 to July 31, 1965
GA-7645	August 1, 1965 to July 31, 1966
GA-8107	August 1, 1966 to July 31, 1967
GA-8787	August 1, 1967 to July 31, 1968
GA-8895	August 1, 1968 through October 31, 1968
GA-9229	November 1, 1968 through January 31, 1969
GA-9359	February 1, 1969 through April 30, 1969
GA-9639	May 1, 1969 through July 31, 1969
GA-9811	August 1, 1969 through October 31, 1969
GA-9838	November 1, 1969 through January 31, 1970
GA-10517	February 1, 1970 through January 31, 1971
GA-10645	February 1, 1971 through April 30, 1971
GA-A10803	May 1, 1971 through July 31, 1971
GA-A10906	August 1, 1971 through October 31, 1971
GA-A12003	November 1, 1971 through January 31, 1972
GA-A12165	February 1, 1972 through April 30, 1972
GA-A12252	May 1, 1972 through July 31, 1972
GA-A12421	August 1, 1972 through October 31, 1972
GA-A12530	November 1, 1972 through January 31, 1973
GA-A12635	February 1, 1973 through April 30, 1973
GA-A12728	May 1, 1973 through July 31, 1973
GA-A12894	August 1, 1973 through October 31, 1973

ABSTRACT

The tasks of the Gas-Cooled Fast Breeder (GCFR) program that are supported by the U.S. Atomic Energy Commission are program planning, core development, out-of-pile heat-transfer and fluid-flow tests, development of a pressure-equalization system for fuel rods, fuels and materials development, and nuclear analysis and reactor physics.

The core development task is to establish criteria for the design of the GCFR fuel, control, and blanket element assemblies. Analytical methods are being developed for predicting fuel-rod response to transient conditions and for treating thermal-hydraulic and structural analyses of fuel assemblies. For the heat-transfer and fluid-flow tests of fuel assemblies, planning of the test program and sizing of the proposed test facility were continued. The development work on the pressure-equalization system included designing the test assemblies for static adhesion tests and seal leakage tests of mating parts, development of the fuel-rod manifold, and development of an analytical model for designing monitoring instrumentation. In the fuels and materials task, the status of the thermal- and fast-flux irradiation programs and analyses of data from these experiments is given. Nuclear analysis and reactor physics work included planning and analytical work for a GCFR critical experiment, surveillance of LMFBR critical assembly experiments, and methods development.

CONTENTS

Figures

Tables

1. INTRODUCTION

The Gas-Cooled Fast Breeder Reactor (GCFR) program sponsored by the U.S. Atomic Energy Commission consists of six tasks: Task 1000—Program Planning, Task 4100—Core Development, Task 4120—Fuel- and Blanket-element Assemblies, Task 4160—Pressure Equalization System for Fuel, Task 4200/4400—Fuels and Materials Development, and Task 4700—Nuclear Analysis and Reactor Physics. The broad objectives of each of these tasks and a summary of the work accomplished in each task during the period covered by this report are given in this section. The technical work performed on the GCFR program during this reporting period is presented in Sections 2 through 6.

The GCFR Utility Program, which is supported by a large number of electric utility companies, rural electric cooperatives, and General Atomic Company, is primarily directed toward the development of a 300-MW(e) GCFR demonstration plant. This utility-sponsored work and the AEC-sponsored work are complementary.

1.1. TASK 1000—PROGRAM PLANNING

This task is primarily to coordinate the planning and implementing of the tasks for the technical development of the GCFR. This task also includes liaison with Argonne National Laboratory (ANL) and Oak Ridge National Laboratory (ORNL) on the safety programs they are performing under AEC funding; the corresponding safety program at General Atomic Company is privately funded.

As this task is primarily administrative, only the technical work performed during this period is covered in this quarterly report.

1.2. TASK 4100—CORE DEVELOPMENT

The objective of this task is the engineering development of the reactor core and associated components. The work on this task is directed specifically to establishing criteria for the design of the fuel- and

blanket-element assemblies. The various analytical and experimental investigations being carried out on this task are reported in Section 2.

Further analytical work on fuel-rod behavior under irradiation conditions in a fast flux has been deferred until the new revision of the LIFE code, LIFE-III, has been issued. A GCFR staff member is participating in the revisions of LIFE as a member of the LIFE Fuel Properties and Models Working Group.

In the analysis of fuel- and blanket-element assemblies, analytical work is being carried out under subcontract by Battelle Pacific Northwest Laboratories on fuel-rod–spacer interactions. This work consists of structural analyses of the spacer grid for several loading conditions imposed by the fuel rod, such as fuel-rod bowing and irradiation-induced swelling and creep, and analyses of the spacer-grid hanger buckling and the spacer-grid mounting. Spacer-grid models are being developed for this analytical work.

Thermal and irradiation distortion of the fuel-element duct is being studied. The analysis uses a detailed model of two adjacent element ducts to determine the hot wall and cold wall temperatures of the duct. The analysis to date has been for the core outlet in an area of large power gradient and is oriented along the core radius between the outer two rows of core elements. Further analysis will be made to determine the convective flow outside the element, the temperature of the element, and the effect of bypass flow between the duct wall and spacer-grid support.

Fuel-rod–spacer interaction tests are being carried out to determine the range of H_2 and H_2O impurities tolerable in the GCFR helium coolant. Fuel-rod cladding tubing and spacer models are tested in helium with various hydrogen-to-water ratios.

1.3. TASK 4120—FUEL- AND BLANKET-ELEMENT ASSEMBLIES

A series of out-of-pile heat-transfer and fluid-flow tests will be performed to demonstrate the ability of the GCFR fuel, control, and blanket element designs to meet design goals and to verify predictions of analytical models that describe design operation and accident behavior.

The test emphasis will be to obtain thermal-structural data for steady-state, transient, and margin conditions using electrically heated rod bundles in a dynamic helium loop. The work carried out on this task is discussed in detail in Section 3.

This test program is to be carried out jointly by GA and ORNL. During this reporting period, an evaluation was performed to establish the basis for the size, power, and flow requirements of the facility. From this evaluation it is recommended that the facility be capable of testing a maximum bundle size of 91 core rods. The test facility that will be used to conduct the heat-transfer and fluid-flow tests will be at ORNL and has been designated the Core Flow Test Facility (CFTF).

1.4. TASK 4160—PRESSURE EQUALIZATION SYSTEM FOR FUEL

The objective of this task is to develop a system for equalizing the pressure between the inside and the outside of the GCFR fuel rod and for venting the fission products via a trapping system and an instrumented activity monitoring system to a helium purification system. The work performed on this task during this reporting period is presented in Section 4.

In the test program for developing the element-to-grid-plate and vent-connection seal, a two-part test program is to be carried out: (1) a materials screening test for determining static adhesion of mated fuel-element and grid-plate parts and (2) leakage tests of vent connection seals. Procurement, fabrication, and assembly of test apparatus and test parts are in progress for both the static adhesion tests and the seal leakage tests.

Analysis of the monitoring system for the pressure-equalization system is being carried out to obtain design information for a system of stations and instrumentation. A Ge(Li) analyzer system is being designed using the computer program COUNT, which is being developed as a monitor-instrumentation design tool. The program will be verified using measured data taken from the capsule GB-10 irradiation experiment using a Ge(Li) detector that is being installed on the gas-sampling line by ORNL.

In the development of a fission-product manifold and fuel-rod support for the fuel elements, design criteria were prepared and applied to a design evaluation of three manifold concepts.

1.5. TASK 4200/4400—FUELS AND MATERIALS DEVELOPMENT

The fuels and materials development and testing program extends and applies Liquid-Metal Fast Breeder Reactor (LMFBR) fuel technology to GCFR requirements. This task includes surveillance of the LMFBR fuels and materials program to utilize existing and developing technology applicable to the GCFR. The status of the GCFR thermal-flux and fast-flux irradiation test programs is presented in Section 5.

Postirradiation of the charcoal trap from irradiated capsule GB-9 continued. Analyses are being made to obtain data on the fractional amounts of the various nuclides deposited in the charcoal trap during operation of capsule GB-9. Analytical determinations of the isotopic contents of the charcoal have been completed and some of the data have been analyzed.

Irradiation capsule GB-10 as of January 12, 1974, had achieved a burnup of 36,200 MWd/Te, of which 27,000 MWd/Te was achieved at 12.0 kW/ft at a cladding outside temperature of 565°C. The capsule is currently being operated at 13.5 kW/ft and a maximum cladding outside temperature of 630°C. Irradiation of capsule GB-10 is continuing at ORNL.

Data on released and vented activity and on iodine release and transport in the GB-10 vented fuel rod have been received. These data are being analyzed at General Atomic. In addition, work has been initiated to install continuous tritium-measuring instrumentation on the sweep-gas line of capsule GB-10.

Irradiation of the seven-fuel-rod capsule experiment F-1 (X094B) has reached a burnup exposure of 65,000 MWd/Te toward a burnup goal of 100,000 MWd/Te on the remaining initial fuel rod (G-4).

Destructive and nondestructive examination of the five fuel rods removed during the second interim examination in early 1973 has been initiated. One of the fuel rods (G-1) has been deencapsulated and diametral

changes determined from profilometry. Analysis of gamma-scanning data taken during the second interim examination continued. The data obtained to date on the volatile species iodine and cesium are presented. Neutron radiographs of rods G-4, G-6, and G-7 confirmed there was charcoal shrinkage in the active charcoal traps in those rods.

The preparation of the fuel rods for the F-3 experiment continued. The assembly of 12 rods was completed. These rods will be encapsulated and sodium-bonded.

1.6. TASK 4700—NUCLEAR ANALYSIS AND REACTOR PHYSICS

This task involves the surveillance and analyses of LMFBR physics work and critical experiments to properly coordinate and develop a GCFR nuclear analysis and physics program and the design and planning of a GCFR critical experiment program. The work performed under this task during this reporting period is discussed in Section 6.

Preanalysis was started on typical matrix cell compositions for the GCFR critical experiment. Using two simple simulation models, a series of homogeneous calculations were performed.

A comparison of ANL and GA diffusion calculations is also continuing. One difference was the upper energy limit used in the two calculations. The ANL upper limit was 10 MeV, whereas the GA upper limit was 14 MeV. The effect of the 10 to 14 MeV range on the GA results is being investigated.

2. TASK 4100—CORE DEVELOPMENT

2.1. FUEL- AND BLANKET-ROD ANALYSIS

Activity during this reporting period consisted of participation in conference calls with members of the LIFE Fuel Properties and Models Working Group. The objective was to obtain agreement on property values and correlations to be used in the next major revision of the LIFE code, LIFE-III. The principal features of LIFE-III had already been established, so the discussions were concentrated on chemical attack of fuel rod cladding, both outside and inside, and on fuel swelling models. The LIFE-III code is scheduled to be issued in March 1974.

2.2. ANALYSIS OF FUEL- AND BLANKET-ELEMENT ASSEMBLIES

2.2.1. Analysis of Fuel-rod—Spacer Interaction

The purpose of this subtask is to perform a structural analysis of the spacer grid structure for several loading conditions imposed on the spacer grid by the fuel rods. These loads result from fuel-rod bowing that is due to temperature gradients across the rods and from irradiation-induced swelling and creep. They consist of both lateral loads and friction-induced axial loads that develop when the rod moves relative to the grid. Battelle Pacific Northwest Laboratories is responsible for the principal effort on this subtask on a subcontract agreement.

The initial model for the axial load analysis consisted of a one-twelfth segment of the spacer grid with constant wall thickness and an axial load applied to each cell of the grid. The grid segment is shown in Fig. 2.1. Each side of a grid cell is represented by a beam element. An initial difficulty was encountered because the model did not provide adequate stiffness to obtain a zero slope at the center of the grid structure. The model was changed to a one-sixth section. This results in a boundary cut that bisects and is normal to each grid beam that is cut.

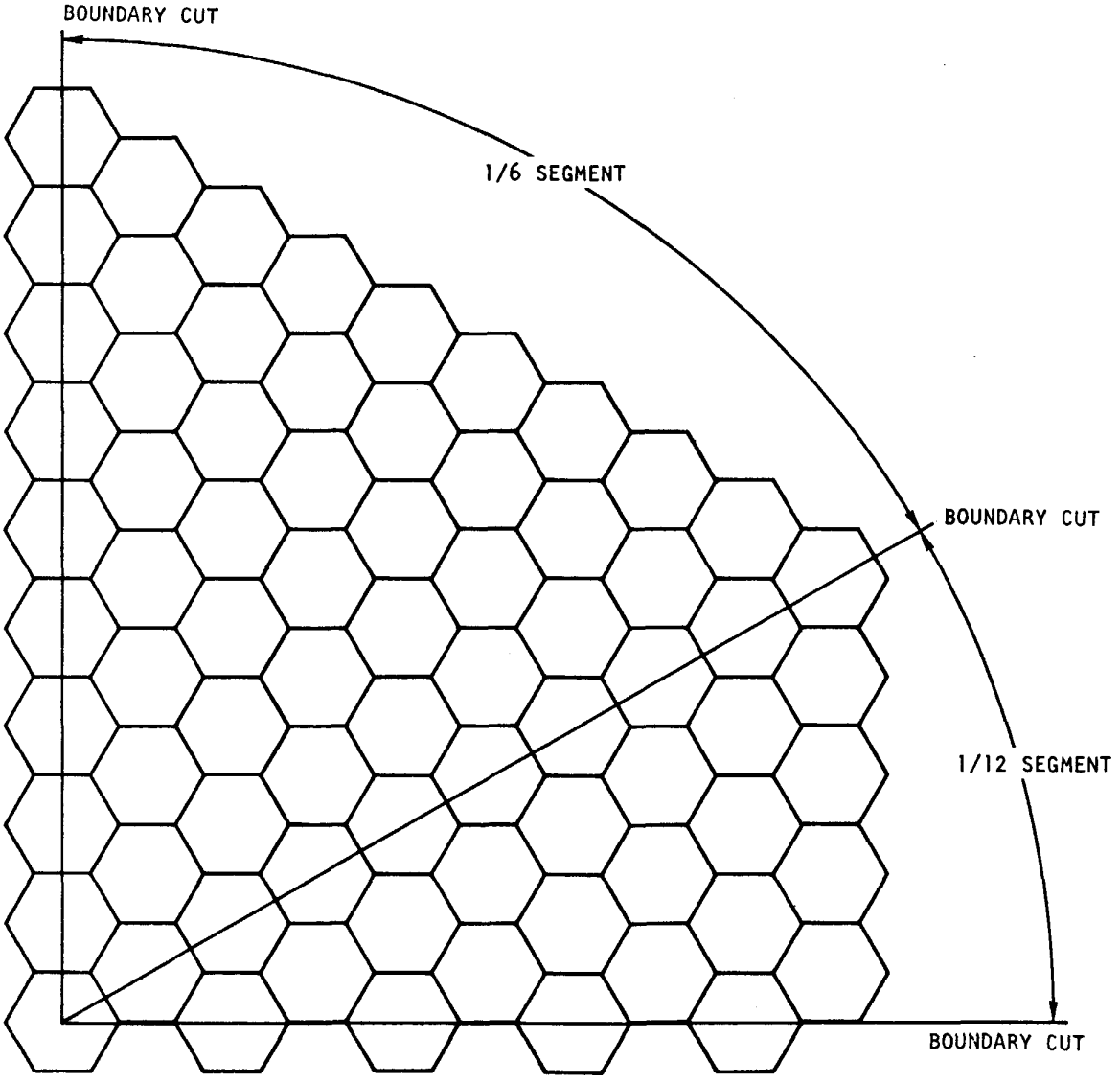

Fig. 2.1 GCFR spacer-grid models

This allows the proper boundary conditions to be applied. Axial load analysis will be continued on the new model.

Evaluation of the spacer-grid hanger buckling has been initiated. This work has shown that it is necessary to lower the weld points on the hanger very close to the fluted section. This is required because the flat upper section of the spacer-grid hanger reduces the buckling-load-carrying capacity because of the low section modulus. An analysis was performed to determine the load-carrying capacity of the spacer-grid hanger for column loading based on inelastic material behavior. Critical column loads and stresses were determined for both eccentric and concentric loading of a column with fixed ends. Thermal and irradiation creep are stress dependent; therefore, it is necessary to iterate the creep deformation and tangent-modulus calculations until a unique stress value equal to the calculated maximum stress for eccentric column loading is obtained. For a temperature of 1000°F and a fast flux of 2×10^{15}nv for 18,000 hr, the allowable column loads and the corresponding stresses were calculated as follows:

	E_e	E_t	E_r
Allowable column loads, lb	380	114	190
Maximum stress (maximum eccentric loading), psi	20,100	6,000	10,000

where E_e = elastic modulus,

E_t = tangent modulus based on elastic and creep strains at 18,000 hr,

E_r = reduced modulus,

$$= 4E_eE_t \Big/ \left(\sqrt{E_e} + \sqrt{E_t}\right)^2.$$

2.2.2. Analysis of Spacer-grid Mounting

The initial purpose of the spacer-grid mounting analysis is to

1. Determine the relative motion of the fuel rods with respect to

the grids to provide a basis for the spacer-grid and fuel-rod interaction tests.

2. Establish a maximum bound on the spacer-grid deflection that could occur due to this interaction.

The analysis also provides an evaluation of the duct-wall temperatures and duct-wall heat transfer with the coolant flow both internal and external to the duct and the spacer-grid hanger. The model used in this analysis also provides an evaluation of the transient bowing motion of the duct.

The model consists of two fuel rods on opposite sides of a fuel assembly and their adjacent flow subchannels, the hanger strap, and duct wall, as shown in Fig. 2.2. Using two fuel rods provides a simulation of power and temperature gradients across the fuel assembly. By coupling the two sides together through the flow channel that is external to the duct, the effect of the external coolant flow and its temperature can also be evaluated. The model consists of eight axial sections. Each side of an axial section, see Fig. 2.3, has an oxide fuel node, two cladding nodes, a hanger node, and a duct node. Each fuel rod has two coolant subchannels and a stagnant helium conductance between the spacer-grid hanger and the duct. (Future modeling will evaluate flow on this stagnant helium region.) Each axial section, therefore, consists of ten thermal capacitive nodes, and thus there is a total of eighty nodes.

The energy balance for each node is written as

$$(\rho c_p v)\frac{dT}{d\theta} = u'''v + \sum_{j=1}^{2} K_j A_j (T_j - T), \qquad (2.1)$$

where ρ = density,

c_p = specific heat,

v = volume,

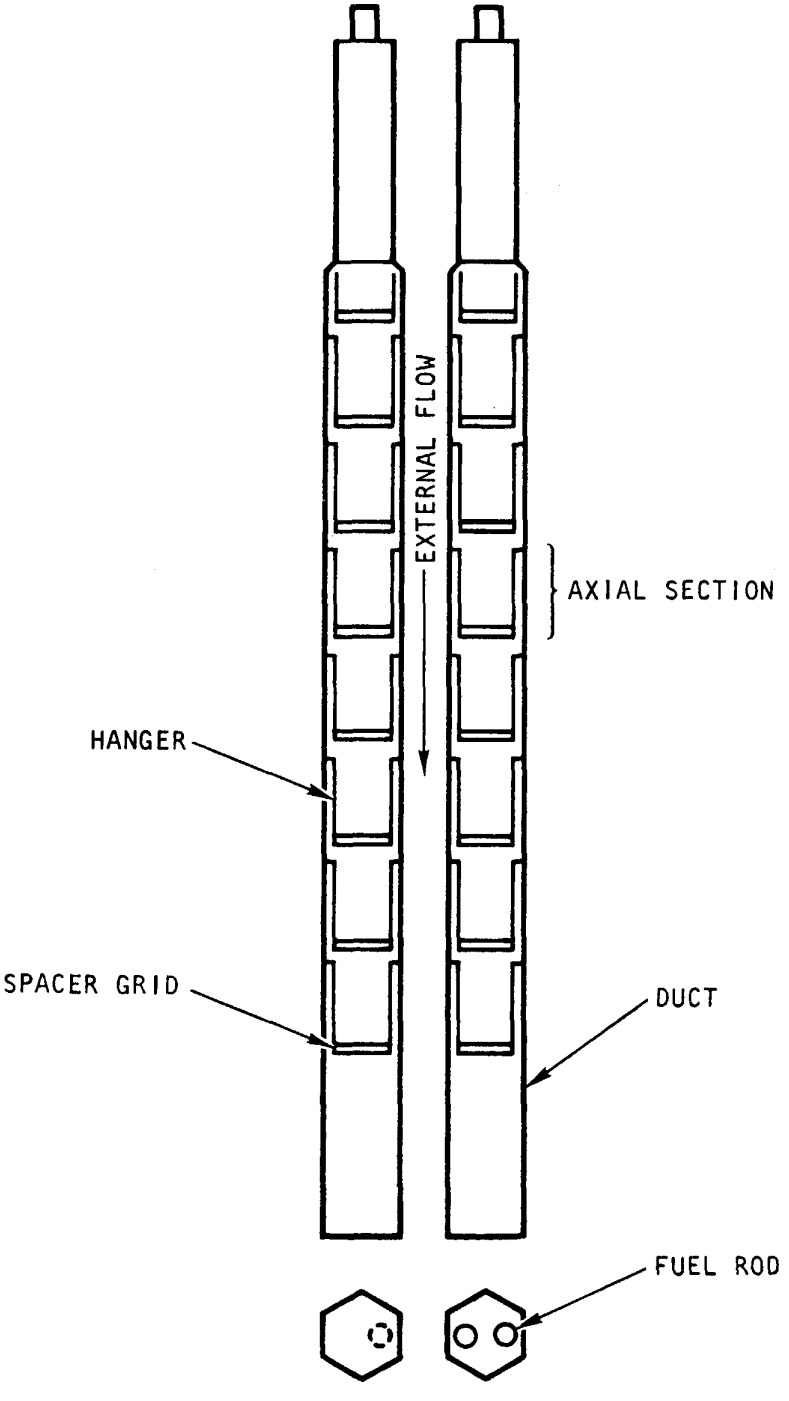

Fig. 2.2 Fuel-rod—spacer-grid interaction model

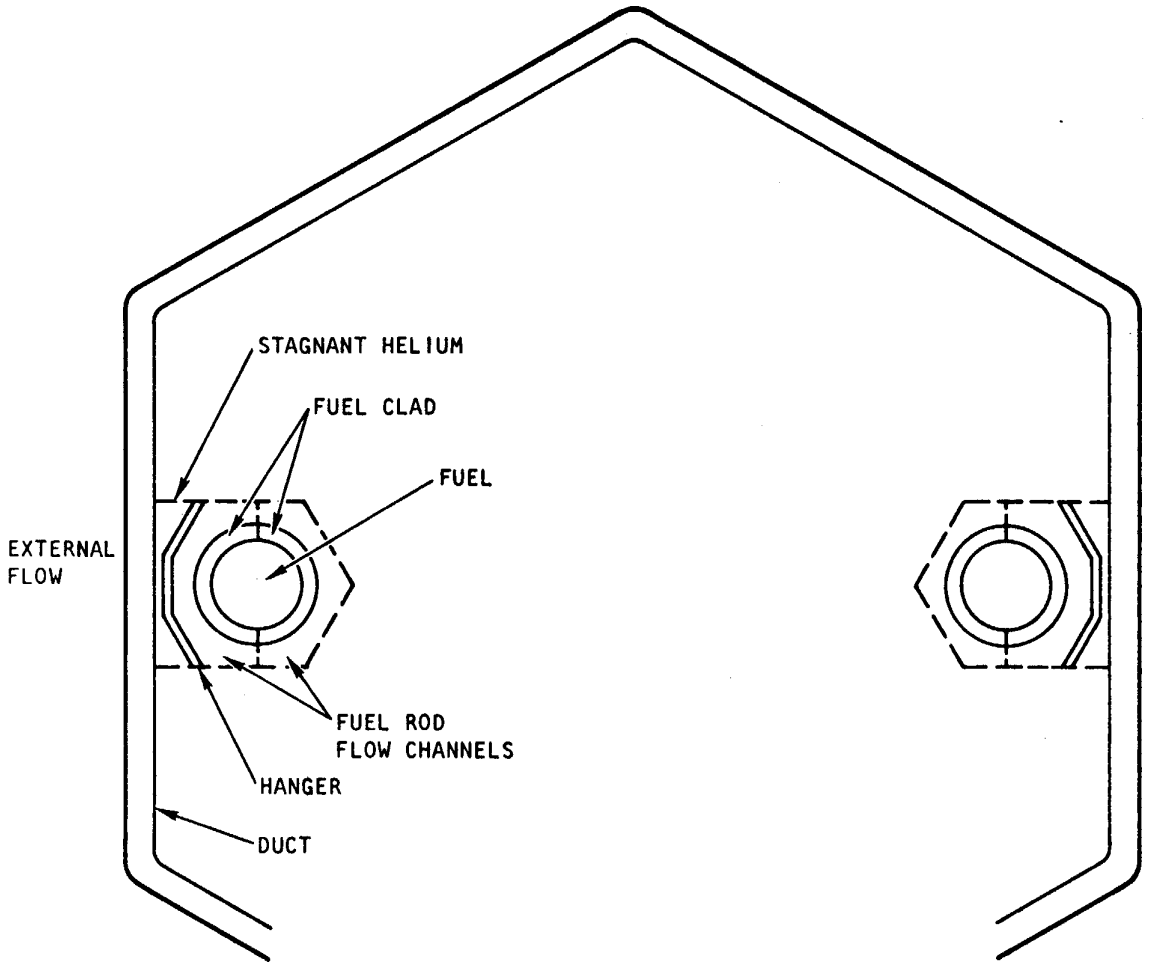

Fig. 2.3 Axial section of fuel-rod—spacer grid model

T = temperature of the node,

θ = time,

u''' = energy generation per unit volume,

A_j = area of heat transfer,

K_j = conductance between the node at temperature T and the neighboring node at temperature T_j (the corresponding area of heat transfer is A_j).

An energy balance for the fluid flowing in each flow channel at a rate m gives

$$(mc_p)(T_0 - T_i) = \sum_{j=1}^{2} h_j A_j (T_j - \bar{T}), \tag{2.2}$$

where T_0 = outlet temperature of the fluid,

T_i = inlet temperature of the fluid,

h_j = heat transfer coefficient associated with area A_j and surface temperature T_j,

$\bar{T}$ = average temperature of the fluid

$= (T_0 + T_i)/2.$

The heat transfer coefficient, h, is calculated from the relation

$$h = \text{ROUGH} \times 0.023 \frac{k}{D_h} (\text{Re})^{0.8} (\text{Pr})^{0.4}, \tag{2.3}$$

where D_h = hydraulic diameter,

k = thermal conductivity of the coolant,

Re = Reynolds number,

Pr = Prandtl number,

ROUGH = increase in h due to surface roughness.

In the range $10^4 < Re < 10^5$, the factor ROUGH is

$$ROUGH = 0.06323(Re)^{0.3}. \tag{2.4}$$

Equations (2.1) and (2.2) form a set of simultaneous equations that are programmed to be solved by a simple explicit procedure.

After the temperatures of all the nodes are evaluated by Eqs. (2.1) and (2.2), the length of each node is given by

$$L/L_0 = 1 + \alpha(T - 72), \tag{2.5}$$

where L = length of the node at temperature T,

L_0 = length of the node at 72°F,

α = coefficient of thermal expansion.

The relative movement between the fuel rod and the hanger at the n^{th} axial node is given by

$$(\Delta x)_n = \sum_{j=1}^{n} L_j - \left(\sum_{j=1}^{n-1} L'_j + L''_n \right), \tag{2.6}$$

where $(\Delta x)_n$ = relative motion between the cladding and the grid at the n^{th} axial node,

L_j = length of cladding at the j^{th} axial node,

L'_j = length of the channel at the node n,

L''_n = length of the hanger at the node n.

The transverse movement of the channel due to the unequal length at the two ends is given by

$$\Delta y = (1 - \cos \phi)R, \tag{2.7}$$

where $\phi = L/r$,

L = length of the colder side,

r = distance between the two sides of the channel,

R = $Lr/\Delta L$,

ΔL = difference in length of the two sides of the channel.

In deriving Eq. (2.7), any thermal stresses induced in the channel have been neglected and it is assumed that the two sides of the channel remain parallel to each other.

Two power and flow transients have been calculated, as shown in Fig. 2.4. The first is representative of a normal coolant-flow coast down. The second is a reactor trip without a coolant-flow coast down. This is an abnormal operating condition that results in a transient thermal shock to the fuel assemblies.

The resulting relative motion of the fuel rod to the spacer grid for each type of transient is shown on Fig. 2.5 for a grid located at the bottom of the fuel assembly. These transients were calculated for a case without a power skew. The relative motion is based on a zero position at 72°F. At steady-state power operation, the fuel rods have moved 0.150 in. from the room-temperature condition. During the transient for reactor trip with flow coast down, the rod moves through a 0.030-in. motion relative to the grid and comes to a new equilibrium position 0.020 in. from the initial power position.

For the case of a reactor trip without a flow reduction, a new equilibrium position is reached 0.130 in. from the initial position. In both cases the new position is reached within 10 to 15 sec of the reactor trip.

Based on the above results, the rod-spacer interaction tests (Section 2.3) have been modified to provide a stroke more representative of the actual transient. The foregoing analysis will be continued to evaluate the effects of power skews to determine bowing transients and evaluate the effect of external duct coolant flow.

2.2.3. Analysis of Element Wall Temperature

The hexagonal duct surrounding each fuel-rod bundle defines the coolant flow boundary for the rod bundle and supports the spacer grids for the rod bundle. The duct is stiff relative to the rod bundle, so element

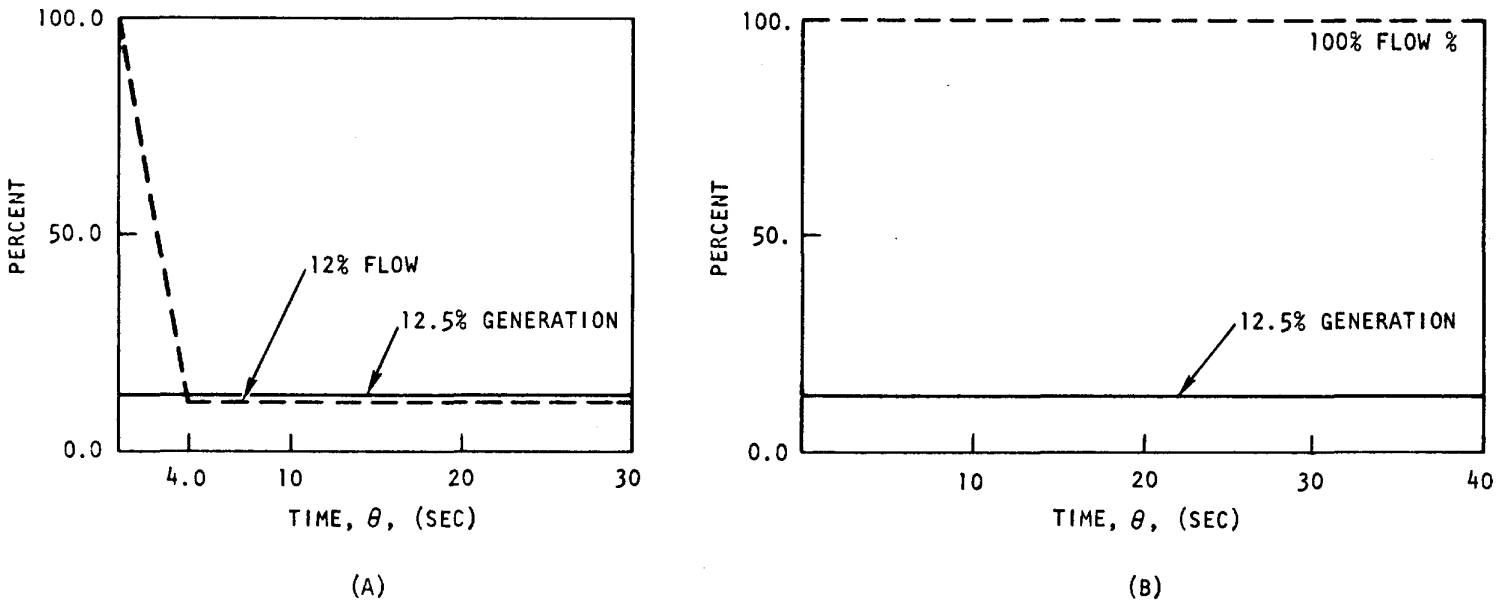

Fig. 2.4 Transients following reactor trip (A) with normal coolant-flow coast down and (B) without coolant-flow coast down

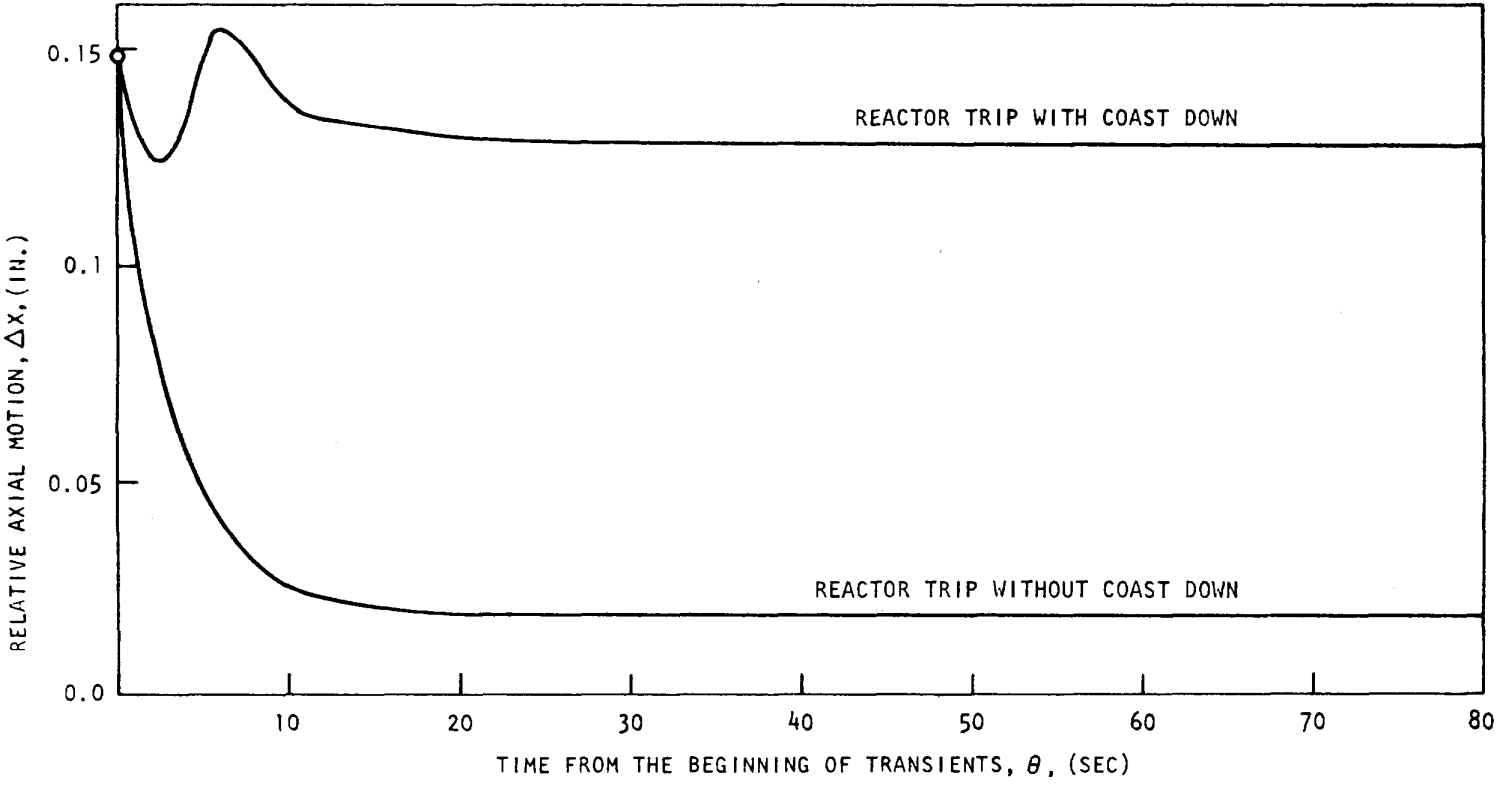

Fig. 2.5 Relative axial motion between the fuel rod and the spacer grid during transients with normal coolant-flow coast down and without coolant-flow coast down and with no power skew

distortion is determined by the combination of thermal and irradiation distortion of the duct. The temperature distribution of a duct directly affects the thermal expansion distortion and indirectly the radiation swelling and creep because of the temperature dependence of these phenomena. In a previous duct distortion analysis, it was assumed that the duct temperature distribution was determined by the temperature of the coolant flowing adjacent to the duct wall within the element and that the local duct wall temperature was equal to the local coolant temperature. This simplification is valid if there is a relatively small thermal resistance between the element coolant and the duct wall and negligible heat flow between adjacent ducts. This assumption tends to overestimate the temperature differences and gradients, which are conservative for the thermal distortion calculations.

The possible error that this assumption introduces is being examined for a detailed model of two adjacent duct walls. The initial model configuration prepared for the TAC-2D[1] heat-transfer code is shown in Fig. 2.6. The model is for a transverse section that includes (1) a portion of a single fuel rod, (2) the associated coolant, (3) the spacer-grid mounting support, (4) the coolant gap between the support and the duct wall, (5) the duct wall and the helium-filled gap between the elements, and (6) the same model items for an adjacent element. The analysis is for the core outlet in an area of large power gradient and is oriented along the core radius between the two outer rows of core elements. The radial power tilt within each element causes a higher temperature at the radial inward side of each element and a lower temperature at the radial outward side of each element. The approximate temperatures for adjacent sides of these outer rows of elements are 900°F and 1100°F, respectively, for the assumption of no interelement heat transfer. With a 200°F temperature difference across a nominal 1/4-in. helium gap, some heat transfer will occur and result in a decrease in the temperature difference because of conduction, convection, and radiation. Convection heat transfer is the major heat-transfer mechanism between elements and is dependent at least on the natural convection that occurs between elements. Leakage across the grid plate or induced flow at the element outlet may cause higher coolant flow. For

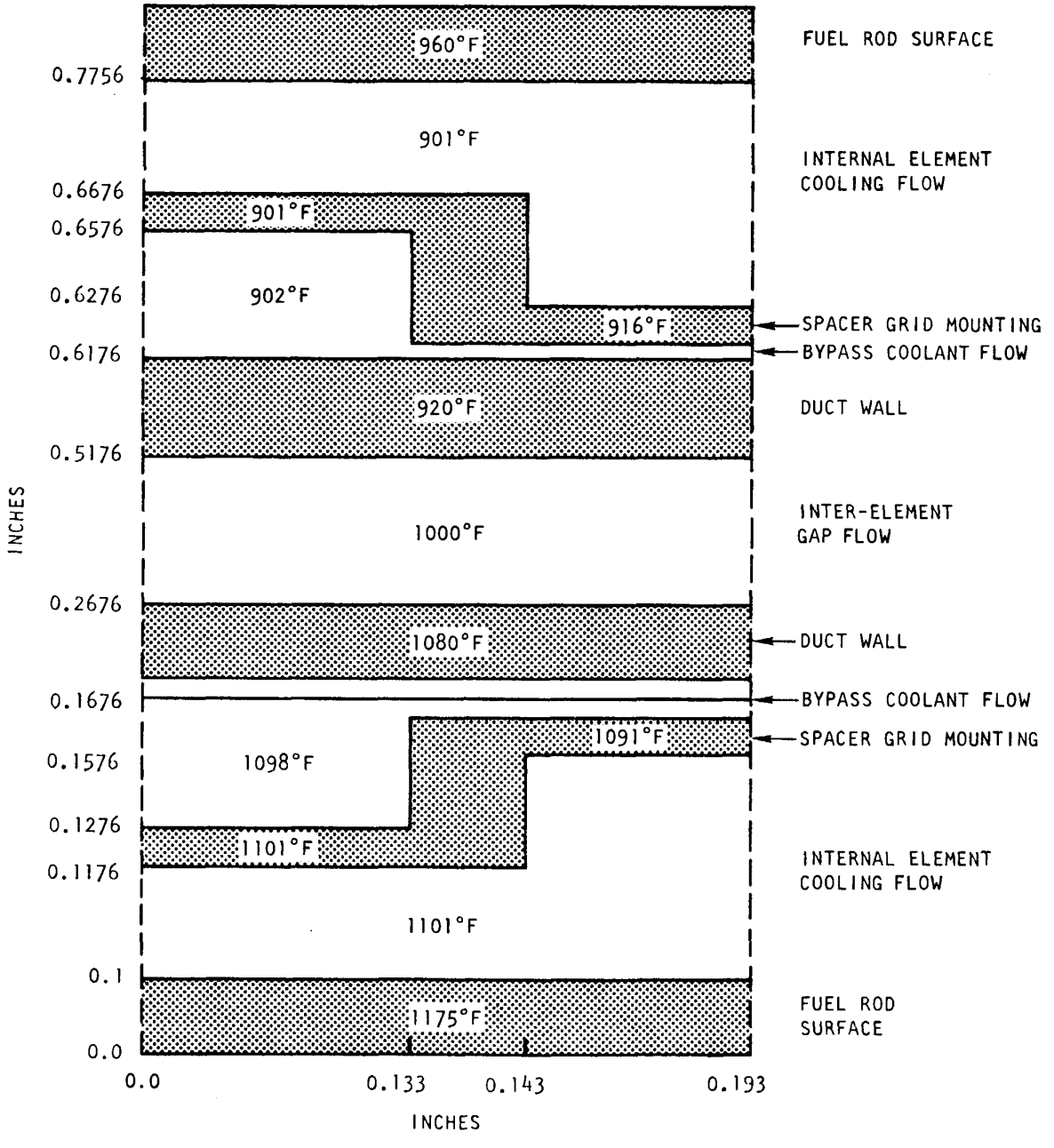

Fig. 2.6 Temperature profiles across the two outer rows of elements

this illustrative analysis, a convection coefficient of 50 Btu/(hr)(ft^2)(°F) is used. The result is that the calculated temperature difference is 160°F rather than 200°F and that the calculated hot wall temperature is (1100°F -20°F) and the cold wall temperature is (900°F +20°F). A refinement in this analysis will determine the convective flow and temperature outside the element and the bypass flow between the duct wall and the spacer-grid support.

2.3. FUEL-ROD–SPACER-GRID INTERACTION TESTS

The objective of the spacer-rod interaction tests is to determine the range of H_2 and H_2O impurities in the GCFR helium coolant for which satisfactory performance of the spacer and fuel-rod interaction can be expected. The intermittent axial motion of the rod relative to the spacer could cause galling, adhesive wear, or metal-to-metal bonding. The contact of the rod and spacer during passive periods could lead to diffusion bonding. In addition, a significant amount of wear would reduce the cladding tube wall thickness and form a notch that could lead to a weakening of the fuel cladding. The degree of these interactions may be controllable by the adjustment of the amount of H_2 or H_2O present in the helium.

The specific experimental objectives are to determine (1) the amount of wear, (2) the coefficient of friction, (3) the appearance of wear or adhering surfaces as a function of impurity content, the normal force, temperature, number and length of the strokes, and the dwell time between strokes. The temperature range to be covered is 325°C to 750°C, which represents a range between the core inlet temperature to 50°C above the maximum hot-spot temperature. This upper temperature was selected to evaluate upper temperature limits for the spacer-rod interaction. Stroke lengths of 1.0-in. and 0.1-in. were selected as being representative of the two types of motion expected—namely, large, less-frequent excursions due to reactor trips and normal shutdowns and small, frequent excursions caused by small power changes. The dwell times between strokes are 1 hr for the 1.0-in. stroke test and 1-min for the 0.1-in. stroke test. These dwell times were chosen to provide the required number of strokes (100 and 4000, respectively) to be accomplished in the test period of 100 hr. Various

H_2O levels in the range of 90 μatm to 4300 μatm are being used. Testing outside this range may be done if definite changes in behavior of the spacer-rod interaction are not observed within that range. Hydrogen-to-water ratios in the range of 10 to 100 will also be evaluated.

Previous test work consisted of seven tests on Type 316 stainless steel tubes with Type 316 stainless steel spacers pressed from 0.010-in. thick strips. All tests were in 900 μatm H_2 and 90 μatm H_2O with a 1-in. stroke length and a 1-hr dwell time. The conditions for these tests are given in Table 2.1.

Table 2.1

INITIAL SURVEY CONDITIONS FOR FUEL-ROD–SPACER INTERACTION TESTS

Test No.	Temperature (°C)	Normal Load (lb)	Surface Condition of Rod
1	750	1.1	Ribbed
2	750	0.35	Ribbed
3,4,7	525	1.1	Ribbed
5	525	1.1	Smooth (rod-spacer couple adhered on 6th stroke)
6	525	0.35	Ribbed

The rods and spacers appeared oxidized after testing, and a wear groove in the ribs was observed. The depth of this groove was approximately one-half the rib height (or 0.003-in.) in Test 1, and it appeared to be about the same depth in other ribbed rods tested. The shape of this groove matched the shape of the dimple on the spacer. In several cases parallel grooves were formed. However, neither changing the side force from 1.1 lb to 0.35 lb nor reducing the temperature from 750°C to 525°C had any significant effect on the coefficient of friction. Spacer thinning was not evident, except for minor surface mars resulting from contact with the rod. The wearing away of the rod ribs is not sufficient to affect the integrity of the fuel rod unless the wear increases by a factor of 2 or

more. The coefficient of friction is larger (see Table 2.3) during the first 10 or 20 strokes, indicating that more wear occurs during the first part of the test. All the tests on ribbed rods ran for the full number of strokes (100).

One smooth rod was tested in the first series (Test 5) and on the sixth stroke the spacer and rod adhered to the extent that a 15-lb axial force could not separate the pair at test temperature. On post-test examination, wear grooves were observed on the rod and displaced metal was located on the rod and spacer surface in the region of contact.

The results of this first test series indicated that the alignment of the test system needed to be improved, that heavier-duty load cells were required in the test rig (10-lb load cells were being used), and that an automatic method of maintaining the water saturator temperature was required. In addition, for test purposes, the lower dimple in the spacer should be removed or not formed initially to avoid possible contact with the bottom surface of the rod that might cause binding of the spacer-rod couple.

The adhesion of the smooth rod and spacer in Test 5 and lack of adhesion when ribbed rods were tested indicated that a more detailed understanding of the behavior of a smooth rod was required. The second test series was planned to determine the effect of atmosphere on the adhesion of a smooth rod and pressed spacers. Test variables held constant were surface condition of the rod (smooth), temperature (525°C), and normal load (1.1 lb). The results are summarized in Table 2.2.

The principal result of this test series was that adhesion of the spacer and smooth rod appeared to be a function of the oxidizing potential of the atmosphere. Preconditioning the samples ~20 hr in the test atmosphere at 525°C or 750°C had no apparent effect on adhesion compared with samples that were not preconditioned. Tests performed with a 0.1-in. stroke and a 1-min dwell time resulted in adhesion when tested in a higher-oxidizing potential atmosphere at about the same total linear travel as did the 1-in.-stroke, 1-hr-dwell tests. Coefficient of friction data are available only for the first of the short-stroke tests because of the erratic performance of the load cells after Test 10. The friction values for that test,

Table 2.2

EFFECT OF TEST ATMOSPHERE AND PRECONDITIONING ON ROD-SPACER INTERACTION
(Smooth Rods, 1.1-lb Load, 525°C)

Atmosphere (μatm)		Stroke Length (in.)	Dwell Time	Test No.	Precondition in Test Atmosphere	Results
H_2	H_2O					
0	90	1	1 hr	8	None	Adhesion
900	90	1	1 hr	9b[a]	20 hr; 750°C	Adhesion
		1	1 hr	12	20 hr; 750°C	Adhesion
		0.1	1 min	10	20 hr; 525°C	Adhesion
		0.1	1 min	11	20 hr; 750°C	Adhesion
9000	90	1	1 hr	14	20 hr; 525°C	No adhesion
		0.1	1 min	13	20 hr; 525°C	No adhesion
20	0	1	1 hr	9a	20 hr; 525°C	No adhesion

[a]Test 9b is a continuation of the 9a test sample in a modified atmosphere.

however, fall in the same range as the values for the long-stroke tests. In general, the length of the stroke or the dwell time do not seem to be significant factors for those lengths that have been tested. The major result of the test series is that control of the H_2-to-H_2O ratio is one method of avoiding adhesion of the spacer and smooth rods.

The third test series was planned to determine the performance of Type 316 stainless steel (SS) and 1.4981 stainless steel tubes, both ribbed and smooth, when tested against 1.4981 spacers, which were electrodischarge-machined (EDM) from 1.4981 SS plate. These materials will be used in the helium-loop irradiation test in the BR-2 Reactor at Mol, Belgium. The test conditions for these tests are: 0.15-in. stroke, 1-hr dwell time, 1.1-lb load, 525°C, 30,000 μatm H_2, and 300 μatm H_2O. The first two tests were performed on smooth tubes, one 316 SS and the other 1.4981 SS. Adhesion did not occur in either test.

The results of the first sixteen tests are given in Table 2.3.

Table 2.3

SUMMARY OF FUEL-ROD–SPACER INTERACTION TESTS

Test No.	Stroke Length (in.)	Dwell Time	H_2 (μatm)	H_2O (μatm)	Temp. (°C)	Normal Load (lb)	Surface Condition	Number of Strokes	Total Linear Travel (in.)	Peak Coefficient of Friction	Coefficient of Friction after 20 Strokes	Notes
1	1	1 hr	900	90	750	1.1	Ribbed	100	100	2.6	0.8	
2	1	1 hr	900	90	750	0.35	Ribbed	100	100	2.6	0.5	
3	1	1 hr	900	90	525	1.1	Ribbed	100	100	1.1	0.6	
4	1	1 hr	900	90	525	1.1	Ribbed	100	100	1.7	1.2	
5	1	1 hr	900	90	525	1.1	Smooth	6	6	1.7	---	5
6	1	1 hr	900	90	525	0.35	Ribbed	100	100	2.2	1.2	
7	1	1 hr	900	90	525	1.1	Ribbed	100	100	(a)	(a)	
8	1	1 hr	0	90	525	1.1	Smooth	8	8	3.1	---	5
9a	1	1 hr	20	0	525	1.1	Smooth	98	98	2.0	0.7	1
9b	1	1 hr	900	90	525	1.1	Smooth	15	15	1.7	---	1,5
10	0.1	1 min	900	90	525	1.1	Smooth	275	27.5	2.7	2.6	1,5
11	0.1	1 min	900	90	525	1.1	Smooth	69	6.9	(a)	(a)	2,5
12	1	1 hr	900	90	525	1.1	Smooth	3	3	3.1	(a)	2,5
13	0.1	1 min	9,000	90	525	1.1	Smooth	4000	400	(a)	(a)	1
14	1	1 hr	9,000	90	525	1.1	Smooth	100	100	3.2	0.6	1
15	0.15	1 hr	30,000	300	525	1.1	Smooth	100	15	1.4	1.0	3
16	0.15	1 hr	30,000	300	525	1.1	Smooth	100	15	(a)	1.5	4

[a]No data due to instrumentation problems.

NOTES:

1. Held ~20 hr in test atmosphere at 525°C prior to test.
2. Held ~20 hr in test atmosphere at 750°C prior to test.
3. 316 SS tube against 1.4981 EDM spacer.
4. 1.4981 SS tube against 1.4981 EDM spacer.
5. Spacer-rod adhesion occurred at stroke number indicated.

A significant difference between the EDM spacers and the pressed spacer is that the surface of the standoff (corresponding to the dimple in the pressed spacer) is a flat surface rather than the convex surface of the dimple. This change in geometry results in the local bearing stress for the flat surface in contact with the rod being less than one-half the stress for the convex dimple in contact with the rod. Additional tests are planned on ribbed tubes and at a higher temperature. This series of tests will not be completed until additional spacers are received and scheduled into the test program.

Better control of the H_2O content in the test gas was achieved by the installation of a mechanical refrigeration system after Test 16. Testing in the second test rig has been deferred due to a delay in receiving the second of the two 25-lb load cells that were ordered early in this period. The load cells have to be paired in each test rig; therefore, substitution of another type of cell is not feasible. Another source of load cells will be found and a pair of cells will be ordered.

Some uncertainty still exists in the water-level readings from the Panametrics probes. These probes are being calibrated and their stability verified. One factor affecting probe performance is the gas flow rate. The current value of 50 cm^3/min may need to be increased to 100 cm^3/min. The Thermox H_2-to-H_2O ratio measuring device has been giving consistently low readings. The correct value of H_2 to H_2O is determined from the known H_2 content of the helium gas and the temperature of the water saturator that determines the H_2O value. The probes and instrumentation will be thoroughly examined and calibrated by Thermox technical personnel.

REFERENCE

1. Petersen, J. F., "TAC-2D-A General-purpose Two-dimensional Heat Transfer Computer Code," USAEC, Report GA-8868, Gulf General Atomic, September 6, 1969.

3. TASK 4120—FUEL- AND BLANKET-ELEMENT ASSEMBLIES

3.1. HEAT-TRANSFER AND FLUID-FLOW TEST

This task was initiated during the previous quarter with the planning of a dynamic helium loop for testing electrically heated rods that simulate GCFR fuel-rod bundles. The development of a heat-transfer and fluid-flow test facility, to be called the Core Flow Test Facility (CFTF), and the prosecution of a test program are necessary to obtain information for the design of GCFR fuel- and blanket-element assemblies. This program includes an evaluation of the operating and safety margins available during steady-state, transient, and accident conditions.

The work on this task is to be carried out under a joint program with ORNL and is being managed by a coordinating committee that represents ORNL and GA. During the previous quarter, the objectives of the program were defined, the areas of responsibility were established, and joint schedules for the overall program and for FY-74 were initiated. The preliminary test requirements are stated in the previous quarterly report.[1] During the current reporting period, an evaluation was performed to establish the basis for the facility size in terms of power and flow requirements.

The CFTF is a high-pressure helium loop in which electrically heated rods will be used to perform experiments on simulated GCFR fuel-, blanket-, and control-element assemblies. The facility will permit tests of the thermal-hydraulic characteristics of these element assemblies under their initial design conditions. The primary objective, however, is to permit the extension of evaluation testing to determine changes in characteristics that occur over the operational life of the elements. The tests, therefore, must simulate the structural interactions that result from both steady-state and transient operational conditions, and the tests must permit the measurement of the effects of these interactions on the thermal-hydraulic performance. These tests will permit the experimental verification of the

design analysis techniques that will be used in predicting the behavior of GCFR-size assemblies. The requirement for simulation of the structural effects has introduced new considerations into the sizing of the loop capability and the power and flow requirements of the loop.

The purpose of this evaluation study was to provide a basis for recommendations on the size of the loop. The evaluation took into consideration (1) the structural and thermal-hydraulic test results necessary to ensure the design adequacy of the fuel, control, and blanket assemblies, (2) the capital and operating cost of the test facility, and (3) the effect of heater-rod reliability on test bundle lifetime. From this, the following conclusions were reached:

1. Simulation of the fuel assembly requires a minimum size of 61 rods to provide an adequate basis for extrapolation of thermal-hydraulic data to full-size GCFR assemblies.

2. Simulation of the control assembly requires a minimum size of 54 rods to adequately simulate thermal-structural interaction of the control-rod guide tube with the fuel-rod bundle.

3. Simulation of the blanket assembly requires 127 rods. This is equivalent to 37 fuel rods, because of the lower blanket power and flow, and therefore does not control the loop capacity.

The minimum requirement of 61 heated rods provides no contingency for the uncertainties associated with this type of experimental program; therefore, it is recommended that the CFTF be designed with a basic provision for expansion to a capacity of 91 heated rods. This increased capacity will provide additional assurance that data can be extrapolated to the full-sized 271 fuel-rod GCFR assemblies. It is uncertain (based on currently available cost data from ORNL) whether the expansion capability from a 61- to a 91-rod size or the initial 91-rod design will be the more economical approach. This determination will be made from a more detailed cost analysis.

Reliability considerations lead to the conclusion that test sections must be designed for replacement of failed heater rods.

3.1.1. Background on Facility Sizing

The CFTF will provide a test bed for out-of-pile model testing o the three types of GCFR assemblies—fuel, control, and blanket assemblies—using electrically heated rods to simulate the fuel rods. The principal test objectives are to verify the design analysis and to ensure that the analysis accurately predicts the performance of GCFR-size assemblies. The testing will include a wide range of operating conditions and effects: steady-state performance, operational transients, upset transients, design basis accident (DBA) transients, margin testing, thermal performance, structural performance, and thermal-structural interaction. The testing will extend beyond the normal steady-state thermal performance now being studied at the Swiss Federal Institute for Reactor Research (EIR) on 37-rod bundles and will concentrate on the thermal-structural interaction associated with transient operation. This requirement for simulation of structural interactions necessitates the use of axisymmetric sections and may be the controlling factor in the determination of bundle size.

In the interest of doing this development task at the least cost, an evaluation of the effect of facility size was undertaken to determine what the minimum size is that will provide the needed technical information. The main variable parameters that affect facility costs are helium flow and electric power input, and these parameters are a function of the test-bundle size. The largest bundle required to complete the needed technical information will set the minimum loop size. However, it is anticipated that for each test, the smallest bundle size commensurate with the objectives of the test will be used.

Each test series requires that the models of the GCFR fuel, control, and blanket assemblies have a particular set of flow, power, and number of heated rods for the simulation. In each case, the structural test requirements necessitate the use of a symmetrical hexagonal array of heated rods. For the fuel assemblies, hexagonal arrays of 37, 61, and 91 rods were considered; for the control assemblies, 1, 2, and 3 rows of rods around the control-rod guide tube require 24, 54, and 90 heated rods, respectively; and for the blanket assemblies, a full-blanket-power 127-rod assembly is

required. The different types of arrays can be grouped together on the basis of requiring approximately the same helium flow and power as shown in Fig. 3.1. Because the power and flow requirements for the blanket assembly are about 10% of those for a fuel assembly, a full-size blanket model is grouped with a 37-fuel-rod model, and thus the blanket test requirement does not affect facility size.

3.1.2. Thermal Considerations on Facility Sizing

The thermal considerations were set on the basis that the primary hydraulic characteristics of a 37-rod bundle under the nominal design conditions at the beginning of life will have been determined under the cooperative program with the Swiss Federal Institute for Reactor Research. These data will permit an accurate description of the behavior in the unperturbed regions of a bundle; however, there still will remain some question about the edge effects and, in particular, the extrapolation of the edge effects for larger bundle sizes. For this reason, it is a requirement to have the capability of going to a bundle size at least one row larger than the 37-rod bundle already being tested, i.e., a 61-rod bundle. This larger bundle size will lend greater confidence in the analytical techniques being used for extrapolation to GCFR-size bundles.

The edge effect is also the paramount thermal-hydraulic effect to be studied in the control elements because those rods and subchannels that are unperturbed are amenable to treatment by the same calculational techniques being employed for the fuel assemblies. As will be seen in Section 3.1.3, two rows of rods surrounding the control-rod guide tube are necessary for simulation of structural effects. The use of two rows of rods, i.e., 54 rods, would permit thermal-hydraulic studies of the effects adjacent to the control-rod guide duct.

As mentioned above, studies of the thermal-hydraulic characteristics of the blanket assemblies require the use of a full-size 127-rod bundle. However, because of the lower power and flow requirements, the blanket assembly does not control the sizing of the loop.

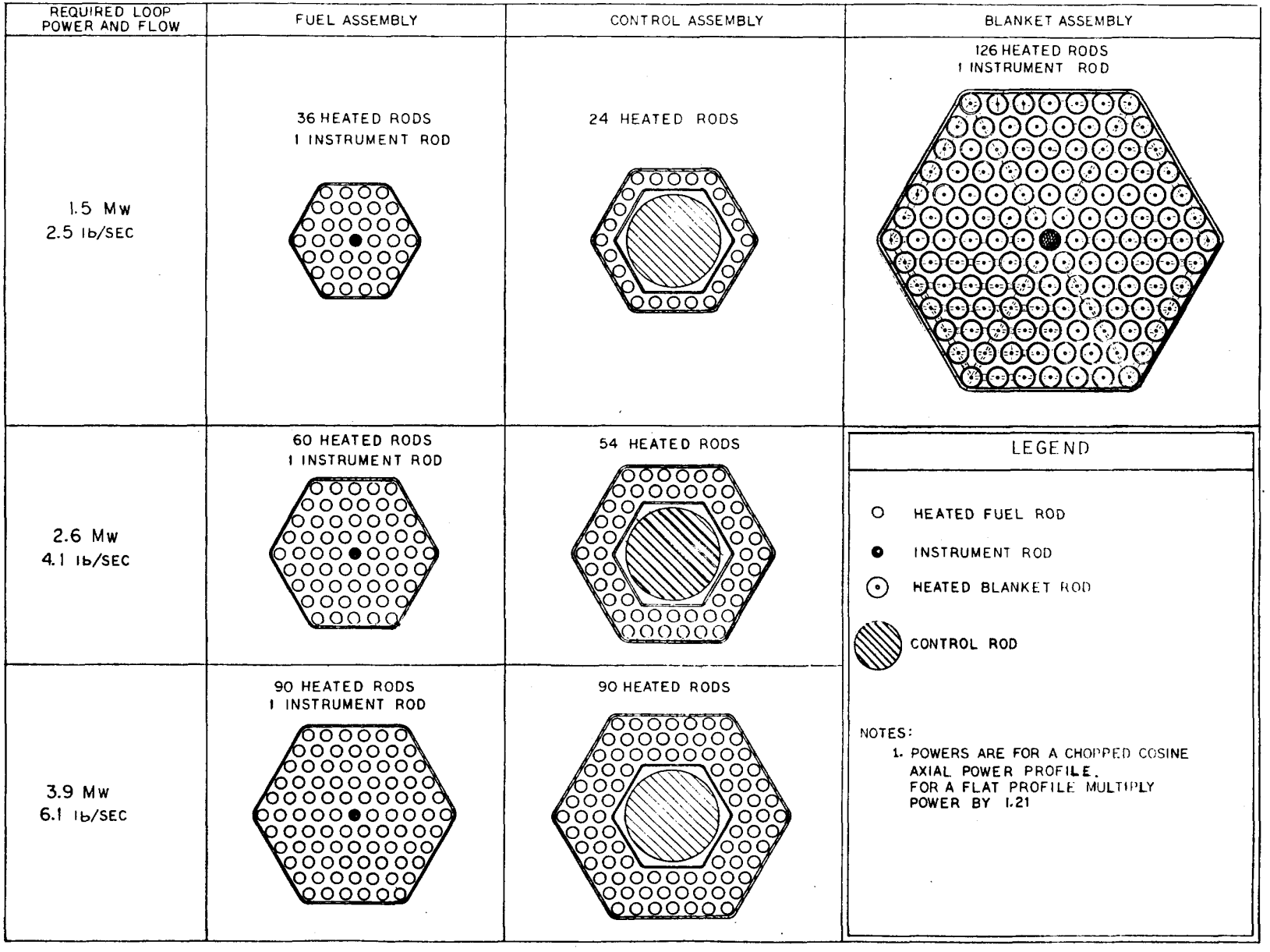

Fig. 3.1 Size comparative grouping of CFTF test sections

3.1.3. Structural Considerations on Facility Sizing

Considerations affecting the simulation of the structural characteristics of the bundles are discussed here. Because full-sized 127-rod bundles will be used for blanket-assembly tests, these tests will be fully prototypic and thus were not considered in the simulation of bundle sizes. The two primary considerations were:

1. Simulation of the radial loading on spacer grids in the control assembly due to differential bowing of the assembly duct and the control-rod guide tube, and
2. Simulation of the spacer-grid deflection under axial load conditions.

The consideration of the differential bowing of the assembly duct and the control-rod guide tube arises from the fact that these two relatively stiff members interact on the spacer grid and the rod bundle. The present design objective is to make the spacer grid stiff enough to resist the forces generated by this differential bowing and prevent distortion of the coolant subchannel geometry. In turn, the radial forces generated between the guide tube and the spacer grid lead to axial loading of the spacer grid as a result of the relative motion between the guide tube and the duct during transient conditions. As it is the effects of both the axial and radial forces that will be studied, the question of simulation focuses on the ability to reproduce forces in the test bundle that are representative of those anticipated in the GCFR-size control assembly.

The analysis of this problem was conducted in several stages:

1. Because the bowing of the ducts is dependent on both the thermal and flux gradients imposed, as a first approximation the flux gradient would be the same across both the assembly duct and the control-rod guide tube. Since the temperature effect of swelling is somewhat second order over the applicable range of temperature, one can consider the effect of swelling on duct bowing to be the same for both the duct and the guide tube and thus is not controlling with respect to spacer-grid loading. The thermal

gradient becomes the controlling factor; therefore, the first step was to apply a thermal-hydraulic analysis using the COBRA-G code to calculate the applicable temperature gradient across the control-rod guide tube. The results yielded a temperature gradient of 25°F/in.

2. The second stage of the analysis applied the CRASIB code to calculate the distortion of the GCFR assembly duct using a temperature gradient of 25°F/in. and thereby define the bowing of the stiffest member of this system.

3. In the next stage, the CRASIB code was applied to calculate the radial loads on the spacer grid when the GCFR assembly duct had the fixed distortion associated with a 25°F/in. gradient, and the gradient on the control-rod guide tube was varied in five stages from 100% to 0% of the 25°F/in. gradient imposed on the assembly duct. The maximum spacer load as a function of the ratio of the assembly-duct temperature gradient to the guide-tube temperature gradient is shown in Fig. 3.2.

4. The final analysis then had the objective of illustrating that in a control-assembly test bundle having two rows of heater rods surrounding the control-rod guide tube, a large enough thermal gradient could be maintained to simulate the estimated maximum load. A 54-rod control assembly test bundle, i.e., two rows of rods around the control-rod guide tube, was therefore studied using COBRA-G. The results of the COBRA-G calculation are shown in Fig. 3.3, where the power factor used for each rod is shown in the circle representing the rod and the outlet temperature of the subchannels is shown in the subchannels. (The calculation assumed half-section symmetry.) The significant observation of these results is that by supplying an opposite power gradient for the outer and the inner rows of rods, opposite temperature gradients across the guide tube and the assembly duct can be maintained, which result in simulated loads on the spacers. Although the differential on the gradients across the two ducts

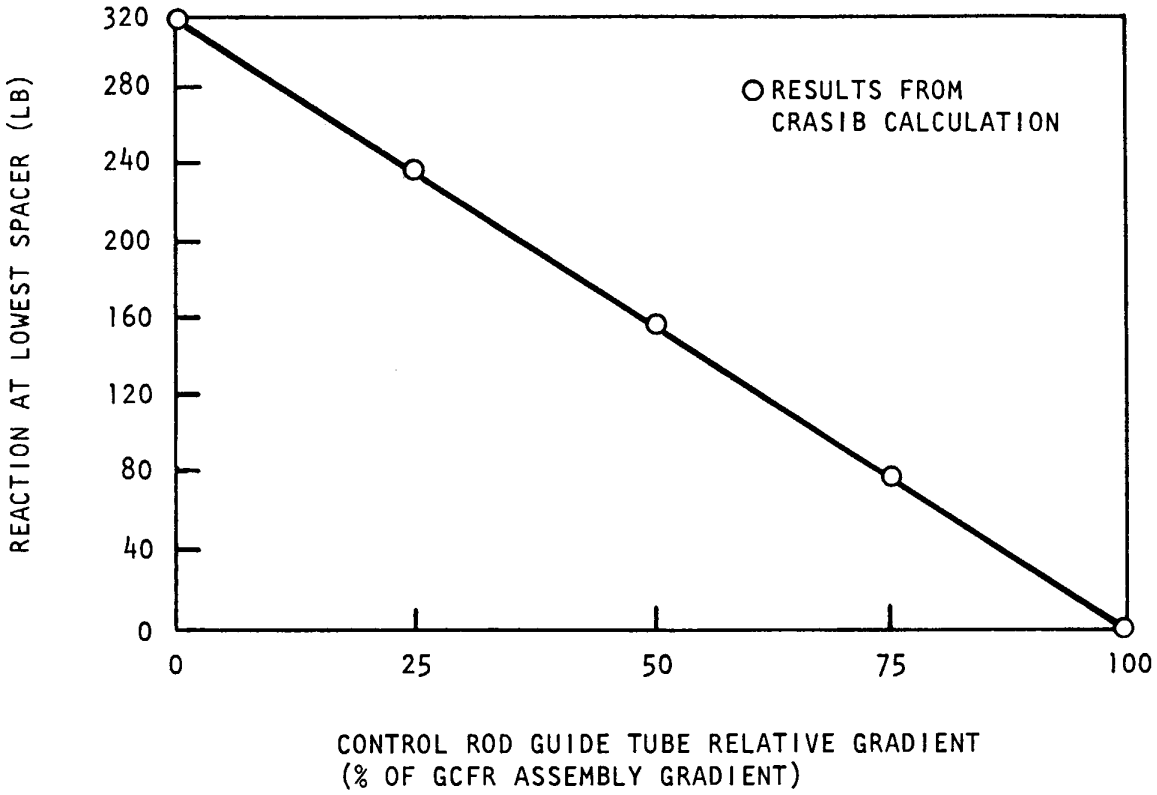

Fig. 3.2 Maximum guide-tube reaction load for duct relative temperature gradient

is ~15°F/in. in this model, a value lower than the 25°F/in. that was used to determine the maximum anticipated load, there is little doubt that a sufficiently large gradient could be obtained by changing the power factors to the rods.

These calculations have established that the loading of the spacer grids can be simulated by a two-row 54-rod model. Furthermore, there is no advantage to be gained with respect to radially loading the spacers by using a larger bundle size.

The second major area of structural considerations was simulation of the spacer-grid deflection under axial-load conditions. Two separate aspects of this have been considered: (1) the displacement of the spacer grid used in a control assembly when subjected to the point loading associated with the spacer grid-duct interaction, and (2) the displacement of

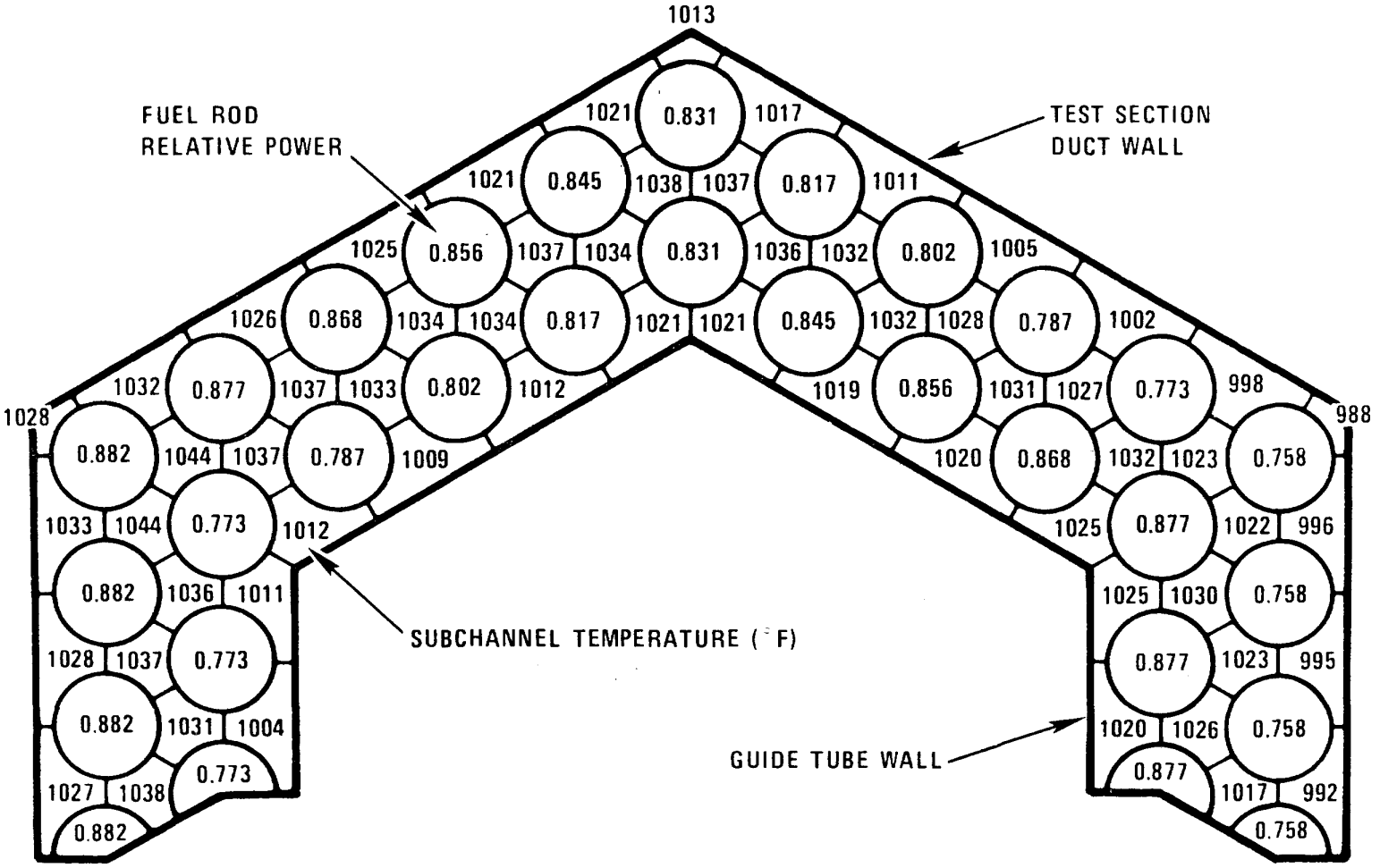

Fig. 3.3 Subchannel temperatures at the exit of a two-row Cobra-G model of the GCFR control element

spacer grids in both fuel and control assemblies when subjected to the uniform loading associated with the interaction between individual fuel rods and the spacer grid. Analyses have been performed of both types of loading in which the spacer was considered as a continuous plate.

The results for the point-loading condition in the control assembly are presented in Fig. 3.4. As shown in Fig. 3.4, with only two rows of rods around the control-rod guide tube, a large fraction (0.7 to 0.8) of the deflection in a full-size assembly is simulated. Increasing the rows of rods would only slowly increase the fraction of the maximum deflection simulated. Therefore, there does not seem to be a large incentive to go to a bundle size having more than two rows.

The results for uniform loading on spacer-grid deflection are shown in Figs. 3.5 and 3.6 for a fuel assembly and a control assembly. In this case, one must go to almost GCFR-size assemblies to simulate a large fraction of the distortion in a GCFR-size assembly. Since it is impractical to consider such large-size bundles, it is apparent that the approach must be to develop analytical structural modeling that (1) can be verified by measurements in these tests and (2) can be used to extrapolate the results to larger-size bundles. From this it can be concluded that uniform loading does not control determination of the size of the bundles to be tested.

3.1.4. Cost Considerations on Facility Sizing

The previous sections concerning thermal-hydraulic and structural considerations indicate that, as a minimum, the loop should be capable of testing fuel-element bundles with 61 heated rods. Owing to the preliminary nature of this study, further analysis and judgment is required to assess whether it would be useful to have the capability of testing even larger bundle sizes. As a first step in making this judgment, a preliminary cost comparison has been made for the facility as a function of bundle-size capability.

The capital cost of the CFTF was estimated by ORNL to be $4 million for a 91-rod facility and $3.5 million for a 61-rod facility. The distribution of the cost was such that only a small fraction of this amount depended on the size of the facility, as can be seen from Table 3.1, in which the details of the costs reported by ORNL are given.

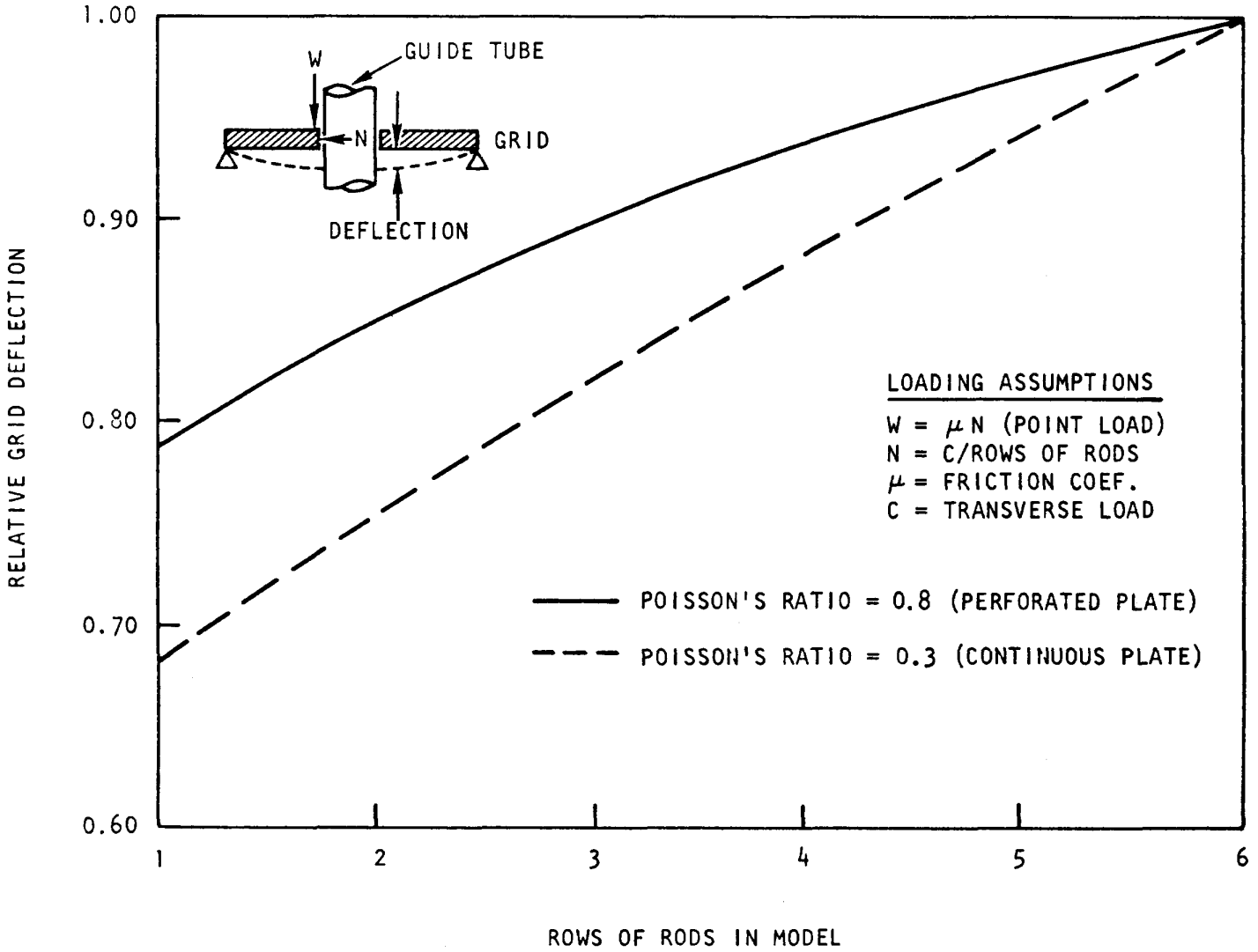

Fig. 3.4 Control assembly grid deflection for model guide-tube friction loads (Deflections are relative to a full size GCFR grid. Model size increases with rows of rods.)

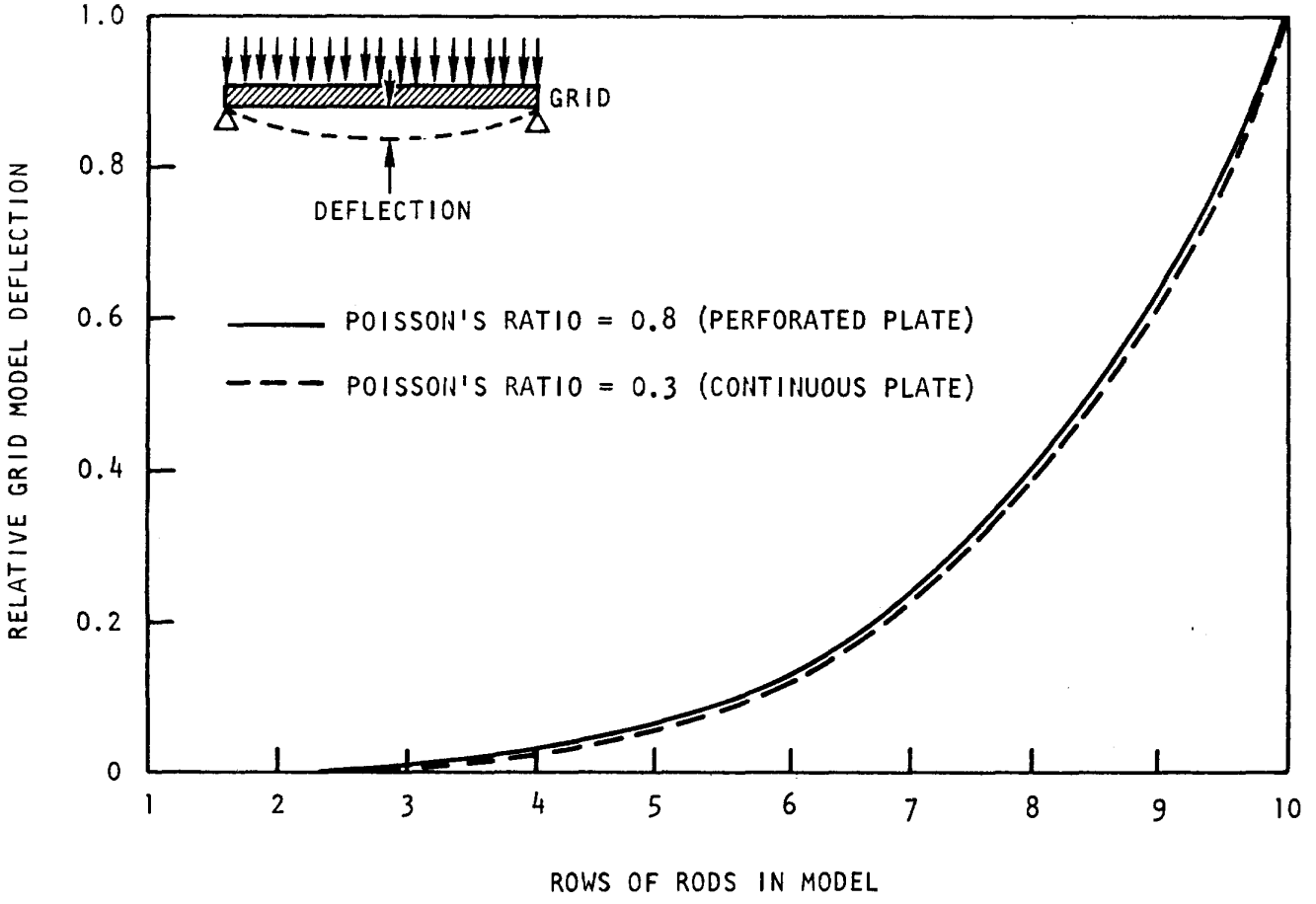

Fig. 3.5 Fuel assembly grid deflection vs. rows in test model (Deflections are relative to full-size GCFR grid. The grid is loaded by a constant amount for each rod. Model size increases with rows of rods.)

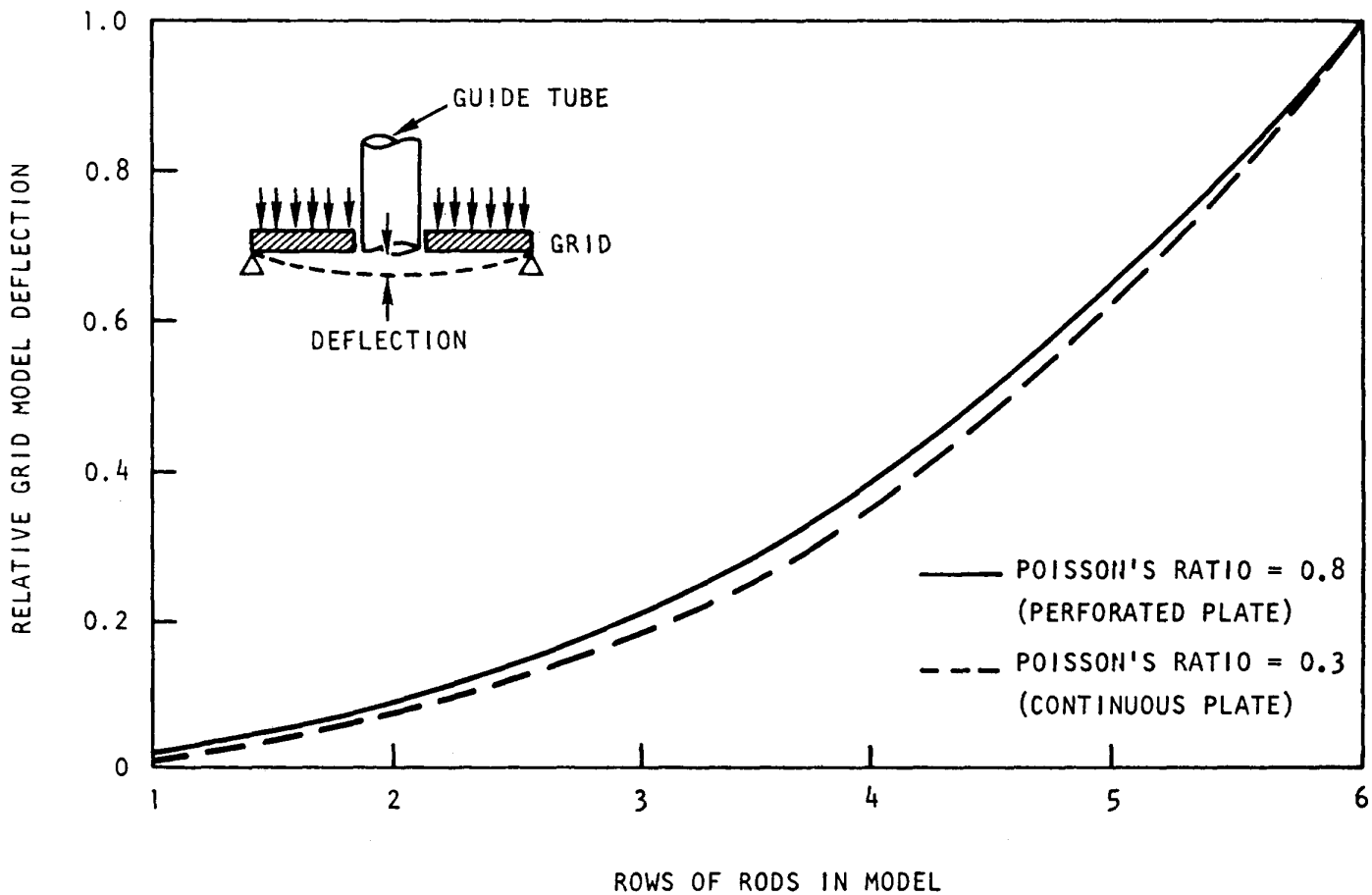

Fig. 3.6 Control assembly grid deflection vs. rows in test model (Deflections are relative to full-size GCFR grid. The grid is loaded by a constant amount for each rod. Model size increases with rows of rods.)

Table 3.1

ESTIMATED COST OF CORE FLOW TEST FACILITY

(in $ thousands)

Size (number of heater rods)	91	61	37
Power, MW	4.1	2.8	1.7
Loop pipe size, in.	6	5	4
Compressor (including spare)	$ 680	$ 600	$ 520
Heat dump	$ 250	$ 200	$ 180
Power supply	$ 330	$ 245	$ 150
Test section	$ 300	$ 240	$ 180
Control room, helium purification system, primary circulation system	$ 750	$ 710	$ 680
Engineering	$ 450	$ 400	$ 350
Contingency (~30%)	$ 770	$ 690	$ 580
Escalation (13.5%)	$ 470	$ 415	$ 360
Totals	$4,000	$3,500	$3,000

The operating costs for the test program based on a 91-rod facility were estimated by ORNL to be $7 million. Recognizing that the operating cost is probably less for a small facility, this amount was prorated to $6.1 million for a 61-rod facility. The total cost difference between a 61-rod and a 91-rod facility was thus estimated to be $1.4 million out of a total of $14 million for the 91-rod facility.

It therefore seems reasonable at this time to recommend that increased flexibility in the program be maintained by constructing a facility with a 91-rod capability. Another possible alternative is to construct a 61-rod facility design that can be expanded to a 91-rod facility without major revisions.

3.1.5. Reliability Considerations on Facility Sizing

There is not a great deal of data relating to the reliability of the present generation of heater rods manufactured under currently applicable quality assurance standards. It is therefore not possible to accurately

assess the relationship between the size of a bundle and the probability that it will operate for the 500-hr design objective with no heater failure. Qualitatively, however, it is clear that bundle reliability decreases as the bundle size increases. Rather than allowing this factor to control the sizing of the facility, it is proposed that the following three steps be taken:

1. The minimum-size bundle consistent with the objectives of a given test should be used for each test.
2. As part of the early objectives of this program, heater quality assurance programs will be developed and reliability data will be obtained.
3. To ensure that the useful life of the bundles is not shortened by heater failure, a design criterion will be the replaceability of heater rods.

3.1.6. Conclusions and Recommendations on Facility Sizing

The conclusions that resulted from this study are:

1. A minimum of a 54-rod capacity is required to simulate the radial loads on the spacer grid in the control assembly.
2. A minimum of a 61-rod capacity is required to test fuel-rod bundles larger than the 37-rod bundles now being tested and thereby permit verification of the analytical models that will be used for extrapolation of bundle test results to GCFR-sized assembles.
3. Testing of a full-size blanket assembly (127 rods) is possible with a loop capacity sized for a 37-rod bundle, and thus it does not control the sizing of the loop.
4. The axial distortion of control-assembly spacer grids due to spacer-duct interactions can be adequately simulated by a 54-rod bundle.
5. The axial distortion of the fuel-assembly and control-assembly spacer grids due to the uniform loading associated with fuel-rod—spacer interaction cannot be simulated without testing bundle sizes approaching GCFR-size assemblies. This means that

instrumentation must be applied to measure the distortion that is attainable and to use these data to verify analytical models that can then be used to extrapolate to GCFR-size assemblies.

6. The absence of reliability data for the type of heaters that will be used in these experiments leads to a requirement for heater replaceability.

7. Preliminary cost estimates indicate no large increase in cost in going from a 61-rod loop capacity to a 91-rod loop capacity.

It is therefore recommended that

1. The minimum-size loop capacity be 61 heater rods.

2. A loop capacity of 91 rods should be considered to allow for uncertainties and to permit a growth capability if it is later found necessary.

3. The 91-rod capability of the loop would most effectively be designed in from the start, but an alternative to be considered is the initial construction of a loop with a 61 rod-capacity that contains an expandable capability to 91 rods.

4. A test-bundle design criterion be established for heater-rod replaceability.

REFERENCE

1. "Gas-Cooled Fast Breeder Reactor Quarterly Progress Report for the Period August 1, 1973 through October 31, 1973," USAEC, Report Gulf-GA-A12728, Gulf General Atomic, December 10, 1973.

4. TASK 4160—PRESSURE EQUALIZATION SYSTEM FOR FUEL

4.1. ELEMENT-TO-GRID-PLATE AND VENT-CONNECTION SEAL TEST PROGRAM

In the GCFR reference design, the fuel, the control, and the blanket elements and their vent connections are sealed to the grid plate by clamping the matching conical surfaces of the elements to the grid plate with a force sufficient to effect a seal and to support the elements, which are cantilevered from the grid plate. These element seals must function at the difference in coolant pressure between the reactor core inlet and exit plenums. There is some uncertainty regarding the effectiveness of the seals over the life of the core. This is caused by the fact that each element may be rotated or relocated several times over its useful life, and because the seals must be effective in a high-purity, high-temperature helium environment while subject to mechanical, vibrational, and thermal effects. In addition, the elements may be subjected to side forces that would tend to disengage them from the clamped contact with the grid plate. Most of the uncertainties are expected to be resolved in a two-part test program: (1) a materials screening test program for prevention of static adhesion of mated fuel element and grid plate parts and (2) leakage tests of fuel element and vent connection seals to the grid plate. Current progress in these activities is given below.

4.1.1. Static Adhesion Tests

The element-seal test program includes a simulation test of small-scale samples of conical seal parts clamped together and tested in a hot helium environment. The test will simulate the conditions of a full-scale fuel element clamped to a grid plate. The design and description of the test is given in Ref. 1.

Procurement, fabrication, and assembly of test apparatus, equipment, and test parts is in progress. Testing will begin in the next quarterly period.

4.1.2. Element and Vent-connection-seal Leakage Tests

The major part of the seal test program is the development and performance evaluation of a full-scale conical element-to-grid plate seal. The design and description of the test and equipment is given in Ref. 1.

The top assembly for vertical clamping of the conical seal parts and the side-loading assembly were lengthened 3 in. to accommodate load cells compatible with GA electronic instrumentation.

Procurement, fabrication, and assembly of test apparatus, equipment, and test parts is in progress. It is planned to procure two sets of element and grid-plate test parts so that the machining changes on one set (angle tolerance and/or finish) can be made while the other set is being tested. Test procedures and test specifications are being written.

4.2. MONITOR-SYSTEM ANALYSIS AND INSTRUMENTATION

The purpose of this subtask is to perform the research and development necessary to provide design information for a system of stations and instrumentation to monitor the activity passing through the pressure equilization system from the fuel and blanket elements to the helium purification system. This monitoring system will measure activity signals resulting from leaks in the cladding of the rods in the fuel and blanket elements, but will reject activity signals arising from exhalation or depressurization. Correlations of signal patterns with the location of cladding leaks and with progressive changes in the conditions of the fuel and blanket elements will be developed.

Basic information on the isotopes (fission products) in the mixtures to be expected under leaking-element conditions will be measured by a Ge(Li) analyzer system that is being installed on the gas-sampling line of irradiation capsule GB-10, which has the unique capability of simulating a leak in an operating fuel rod in an element.

The Ge(Li) analyzer system is being designed with the aid of the computer program COUNT, which is being developed as a monitor-instrumentation design tool. Options for the Ge(Li) detectors and collimators

have been written into the program, as described in the previous quarterly report.[1] The COUNT program will subsequently be modified and then verified using the measured data obtained for various simulated leak conditions in the GB-10 irradiation experiment.

The analyzer design must result in adequate counting rates for both the "no leak" (sweeping across the top of the trap) and the "leak" simulation (sweeping through the fuel, blanket, and trap) flow modes without saturating the detector. This has been parametrically studied with variables of collimator size, separation distance, sample-line size and gas flow rates.

Analyses using the COUNT program were continued. A satisfactory general configuration and arrangement for the Ge(Li) analyzer has been found that required reducing the sample-line-to-detector separation distance to 381 mm and increasing the radioactive gas volume in the area of the analyzer by enlarging the sample-line tube into a 5.8 mm-diam source chamber. Adequate counting rates were obtained using existing collimators at ORNL that are 305 mm thick and have hole diameters of 6.35 and 25.4 mm for the flow modes in through the bottom of the fuel and out through the top of the trap and in and out through the top of the trap, respectively. The variation in photopeak counting rate, as computed with COUNT, is shown in Figs. 4.1 and 4.2 as a function of the sweep-gas flow rate for each fission product expected to be present in the gas in the "no leak" and "leak" simulation flow modes, respectively. These results define the general design and configuration of the Ge(Li) analyzer and complete the work to be done at GA. The detail design, installation, calibration, and operating verification of the analyzer are being done at ORNL under a subcontract.

To accommodate the design requirements and to develop a practical design configuration for the analyzer for capsule GB-10, ORNL has provided space in a nearby cubicle in which to install the analyzer. A bypass sweep-gas line from the shielded valve box will conduct the gas to the counting source chamber. During shutdown of the ORR in November 1973, valving for the bypass line to the analyzer was installed. Installation of the bypass line between the valves is planned during the next refueling shutdown of the ORR.

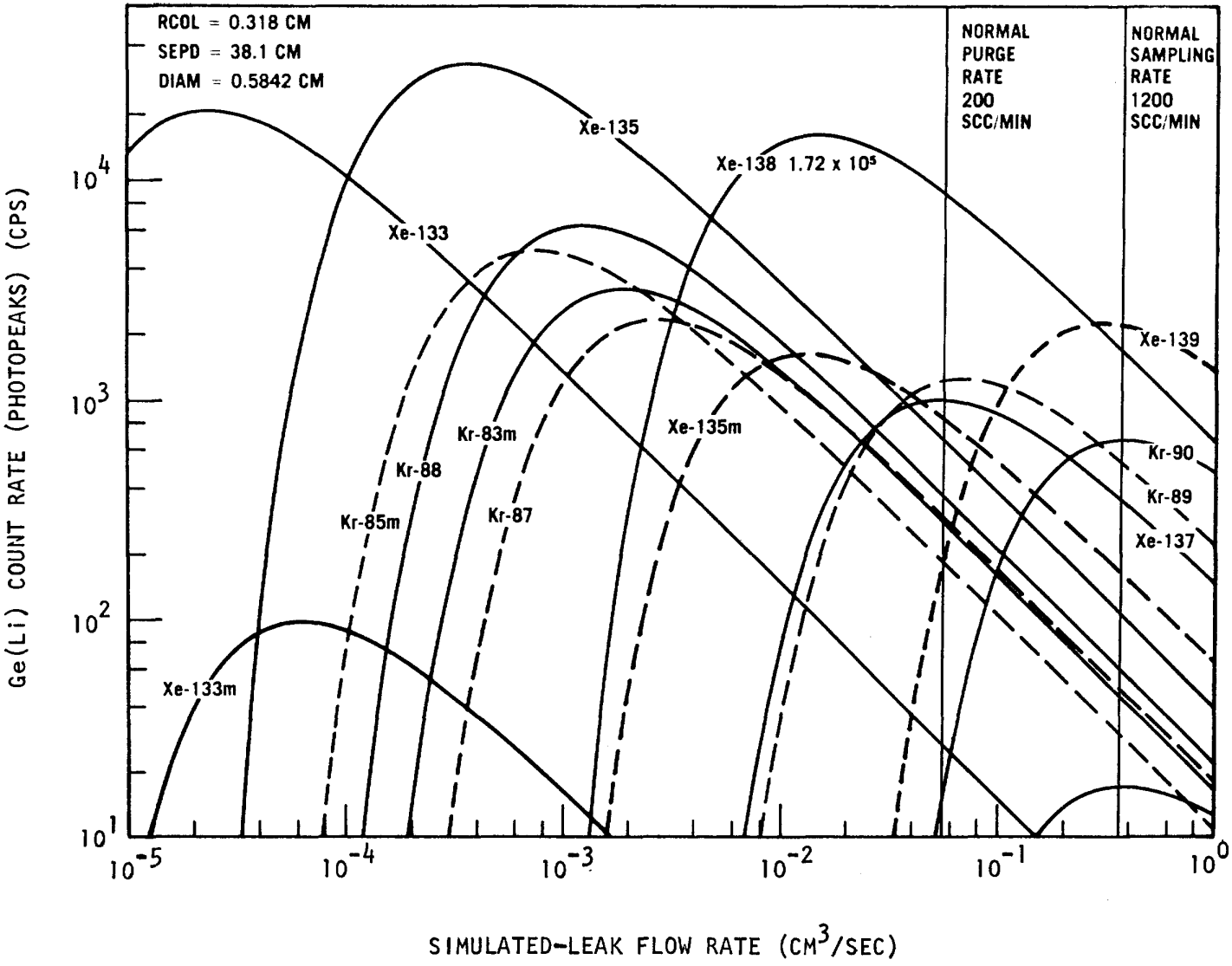

Fig. 4.1 Simulated-leak flow rate in capsule GB-10 in flow mode in through the bottom of the fuel and out through the top of the trap.

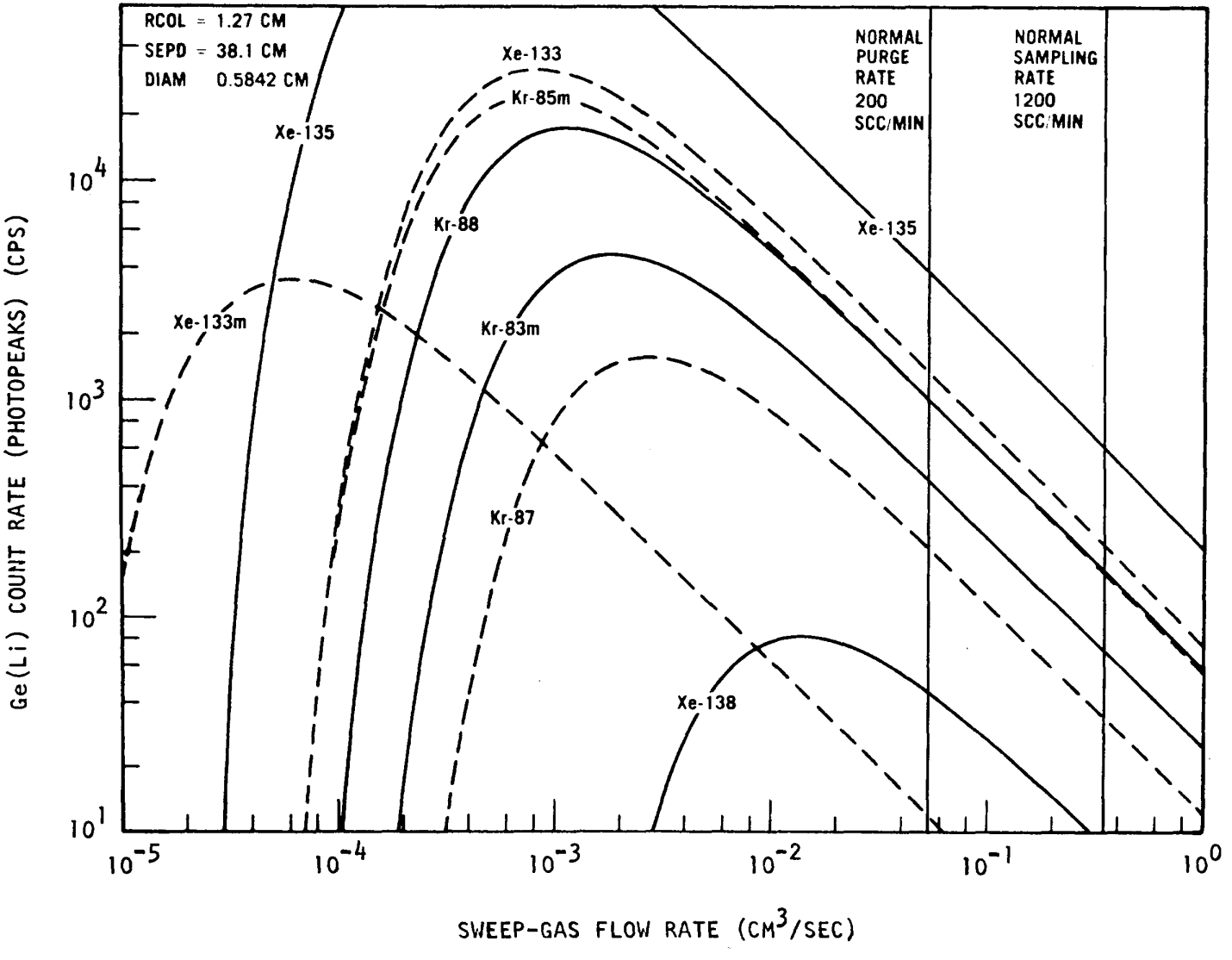

Fig. 4.2 Sweep-gas flow rate in capsule GB-10 in the flow mode in and out through the top of the trap

It was decided that the counting source chamber should be made of aluminum so as to suppress the bremsstrahlung background radiation. Also, the chamber would then be rugged enough for handling without substantially attenuating the gamma radiation.

The performance of the Ge(Li) detector was checked before it was shipped to ORNL and a resolution of only 4 keV was obtained, compared to a rated value of 2.3 keV (FWHM). A resolution of ~3.0 keV was measured at ORNL after the detector was received. If further improvement in the resolution is needed, ORNL plans to supplement this detector with a portable one of higher resolution whenever better resolution of the gamma peaks in the spectra is indicated.

4.3. FUEL-ELEMENT FISSION-PRODUCT MANIFOLD

The design criteria for the fuel-rod support and fission-product manifold were completed. They were applied to a design evaluation of three manifold design concepts. The design concepts are briefly described below:

1. The first concept of the GCFR fuel-element manifold reference design is shown in Fig. 4.8 of Ref. 1. This design combines the fission-product venting function and the rod support function into a single-level manifold.

2. The second concept is shown in the design layout in Fig. 4.3. This is a two-level design, with each level handling both functions of fission-gas manifolding and fuel-rod support. A tube connects the two levels for passage of the fission products from the lower level of fuel-rod connections to the upper level of fuel-rod connections.

3. The third concept is one that separates the fission-product manifold function from the fuel-rod support function. One design layout concept of this is shown in Fig. 4.4. Each fuel rod has a vent tube connection to the element annular trap. The fuel rods themselves are screwed into the top grid for support only. The fuel-rod vent tubes are welded into the lower plenum of the element charcoal trap.

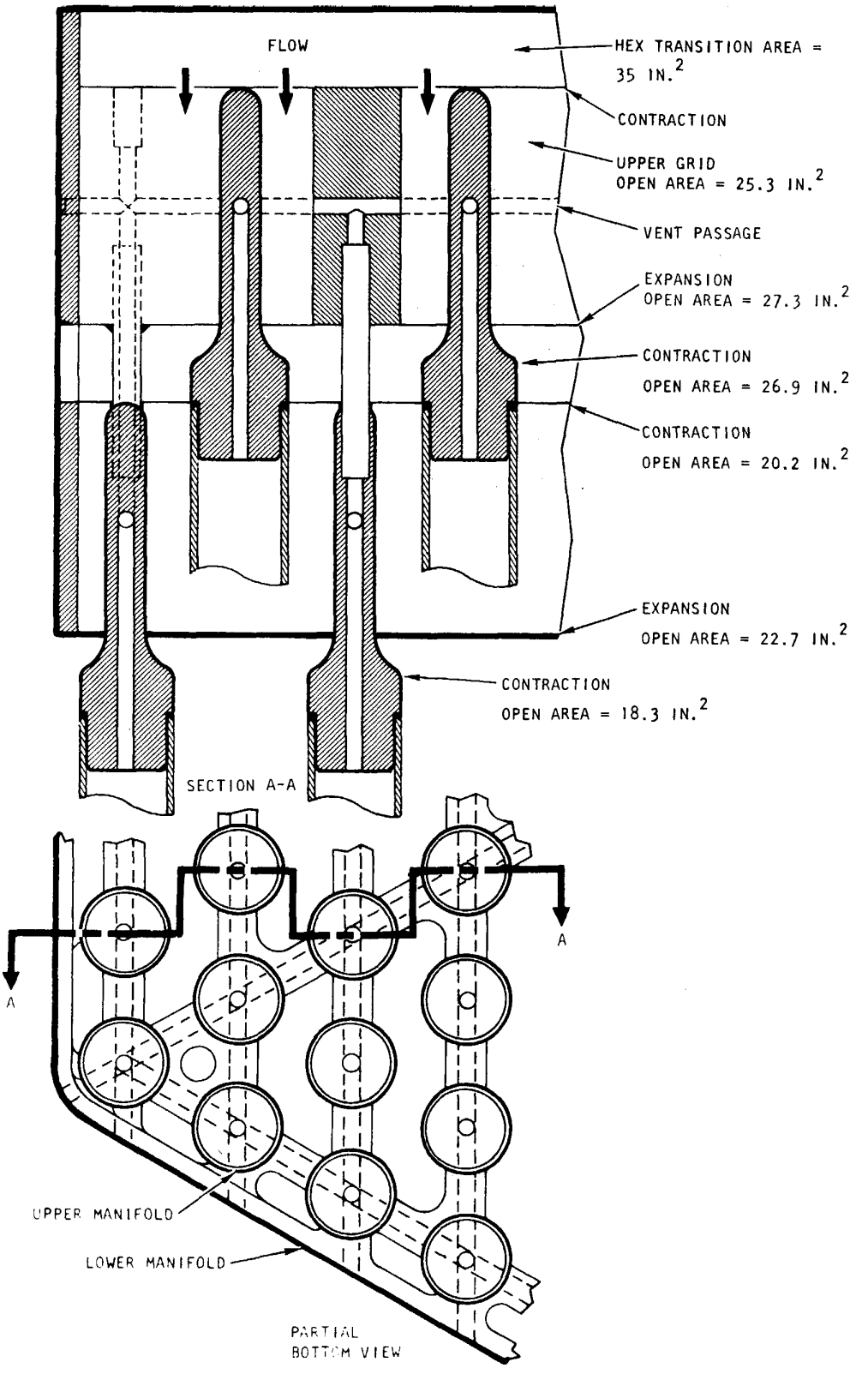

Fig. 4.3 Two-level fission-product manifold and support grid

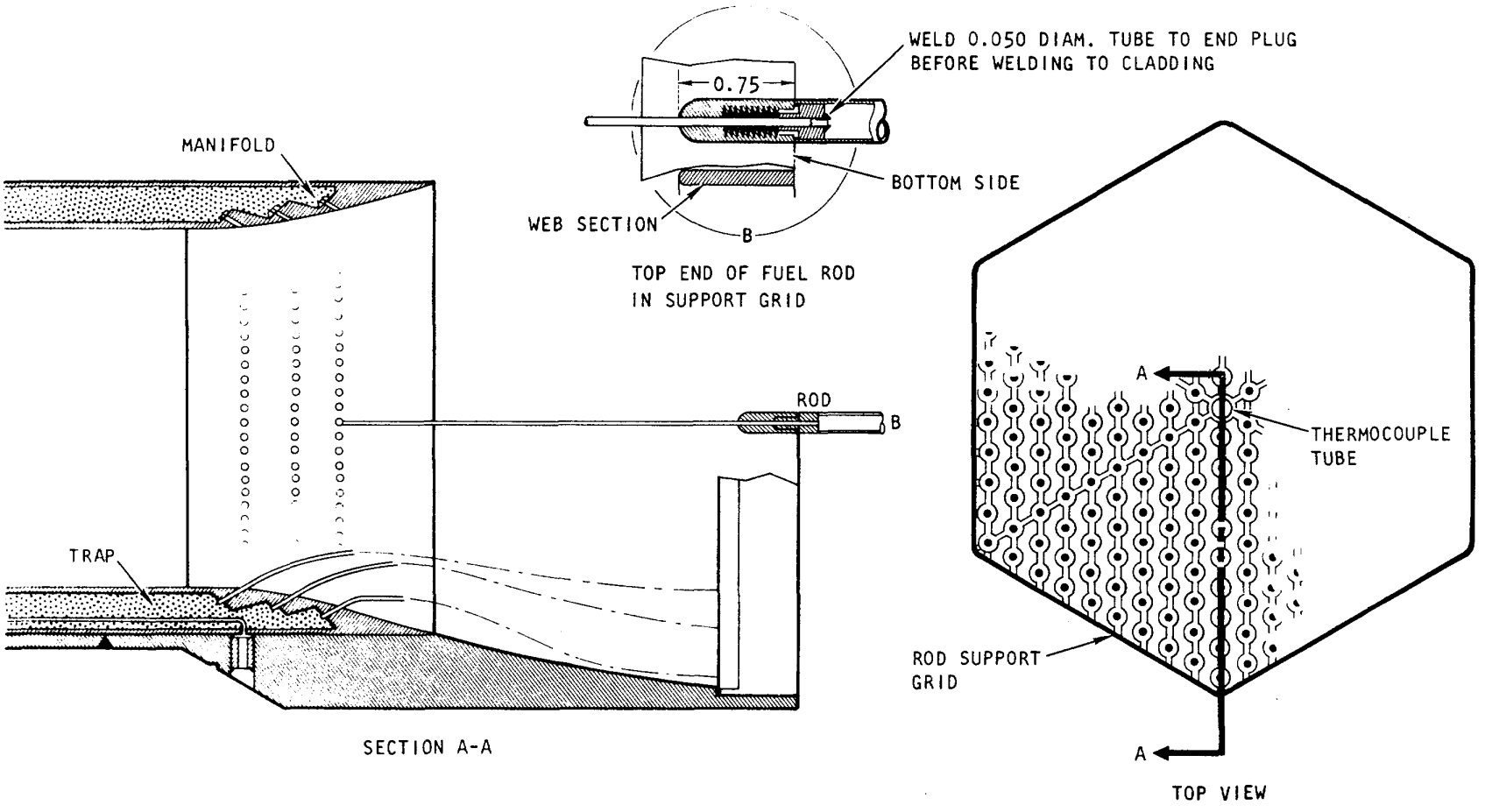

Fig. 4.4 Tubular vent fission-product manifold and separate rod-support grid

Each concept is being studied in the design evaluation to determine if the design criteria are met. The general criteria being evaluated are:

1. Coolant-flow pressure drop,
2. Structural adequacy,
3. Material adequacy for the thermal and irradiation environment,
4. Fission-gas venting redundancy,
5. Fabricability,
6. Feasibility of inspection, and
7. Fuel-rod sealing requirements.

The design evaluation has considered the first two criteria given above. The stated design objective in the criteria for the coolant pressure drop across the fission-product manifold is 1.5 psi out of a total of 6 psi established for the total fuel-element inlet loss, including the manifold. Thus, the manifold pressure loss would be limited to 25% of the element inlet loss. A comparison of estimated inlet pressure drop for the three concepts is given in Table 4.1. The values in Table 4.1 are based on contraction, expansion, and tube-flow friction coefficients given in Refs. 2, 3, and 4. The straight-tube friction pressure losses are probably accurate to 10% to 15%. The literature survey given in Ref. 3 indicates good agreement on expansion losses where the expansion coefficient is related to the area change as follows:

$$\Delta P_{ex} = K_e \frac{\rho V_1^2}{2g},$$

where

$$K_e = 1 - \left(\frac{A_1}{A_2}\right)^2,$$

V_1 = velocity at inlet area A_1,

ρ = average coolant density,

A_1 = expansion area.

There is less agreement on the contraction losses because it is greatly dependent on the inlet shape and the Reynolds number. For a well-rounded tube inlet, the contraction loss is negligible. The contraction coefficient for slotted entries as a function of area ratio and Reynolds number are given in Ref. 4. The use of these values to calculate the contraction pressure losses given in Table 4.1 is conservative.

Table 4.1

ELEMENT INLET PRESSURE LOSS
(psi)

Pressure Loss Areas	Integrated Venting		Separated (Tubular) Venting
	Single Level	Two Levels	
Inlet structure expansion	0.02	0.02	0.02
Trap contraction	0.15	0.15	0.15
Trap friction	0.04	0.04	0.04
Hexagonal-duct transition	0.76	0.76	0.73
Hexagonal-duct friction	0.02	0.02	0.3
Top grid support contraction	0.12	0.05	0.10
Top grid support expansion	0.21	0.01	0.21
Lower grid support contraction	---	0.07	---
Lower grid support expansion	---	0.08	---
Total element inlet pressure drop	1.32	1.20	1.55

The definition of flow geometries for the second and third concepts (Figs. 4.3 and 4.4) is quite complex (i.e., the flow between the upper and lower grids of Fig. 4.3 and the flow across and parallel to the vent tubes of Fig. 4.4). Because of this, a higher uncertainty of 25% to 30% has to be applied to those complex flow-region pressure losses.

Because of the large calculational uncertainty in the separate venting estimates, it is concluded that all three concepts will result in a pressure drop of less than 1.55 psi and in a total pressure drop from the element inlet to the fuel-rod bundle of considerably less than the

6 psi allowable. Thus, all three manifold-support concepts appear to satisfy the criteria for coolant pressure loss. It would also appear that the two-level manifold would result in the lowest inlet coolant pressure loss, although this advantage is not highly significant compared to the total system pressure drop.

An evaluation of the second criteria—structural adequacy—is being made but has not been completed. The normal static loads to be considered are:

1. The weight of the fuel rods, which is about 1.5 lb per rod.
2. The coolant flow forces on the manifold structure, which total about 10 lb, or less than 0.05 lb per rod.
3. Coolant-flow friction forces on the fuel cladding of about 5 lb per rod.
4. Potential friction forces from interaction of bowed fuel rods with the spacer grids that would result from different thermal expansion and irradiation swelling. These forces could amount to nearly 10 lb per rod.

The total static forces on the spacer grid due to the loads indicated above are about 4000 lb. On any cross-structure member, this results in a total distributed beam load of about 300 lb, or a maximum of about 50 lb/in. The dynamic loads are those due to vibration and seismic forces induced directly on the manifold or transmitted from other structures.

The materials selected for the manifold structure are the 300 series stainless steel (Type 304 or 316). The fluence level is less than 10^{21} nvt ($E > 1$ MeV) at the manifold. Thus, these stainless-steel materials should not have to be cold-worked, since irradiation swelling is negligible at fluence levels below 10^{22} nvt. Also, the operating temperature of ~300°C does not pose any problem for these materials. The study of materials adequacy in the design evaluation is being continued.

The design evaluation is continuing on the other criteria listed above. For each design concept there are variations in details, such as fabrication techniques for the fuel-rod connection seals, that must be included in the studies.

REFERENCES

1. "Gas-Cooled Fast Breeder Reactor Quarterly Progress Report for the Period August 1, 1973 through October 31, 1973," USAEC, Report Gulf-GA-A12728, Gulf General Atomic, December 10, 1973.

2. Schutt, A., "Losses of Pressure Head Due to Sudden Enlargement of a Flow Cross-Section," ASME, HYD-51-10, 1929.

3. Armstrong, R., "Pressure Loss in Piping Systems; a Comparison of Conventional Factors for Fluid Friction in Piping Components," USAEC, Report AECU-454, Argonne National Laboratory, August 1961.

4. Hamilton, J., "Suppression of Pipe Intake Losses by Various Degrees of Rounding," Bulletin No. 51, University of Washington for Engineering Experimental Station, 1929.

5. Kays, W., and A. London, Compact Heat Exchangers, McGraw Hill Book Co., Inc., New York, 1958.

5. TASK 4200/4400—FUELS AND MATERIALS DEVELOPMENT

5.1. THERMAL-FLUX IRRADIATION EXPERIMENTS

5.1.1. Irradiation Capsule GB-9

Postirradiation examination of the charcoal trap from the GB-9 irradiation experiment continued during the quarter. The analyses were directed toward obtaining data on the fractional amounts of the various nuclides deposited in the charcoal trap during the operation of the GB-9 experiment. These fractional amounts are expected to vary, depending upon the chemical form (gas or volatile) of the released nuclides and their respective half-lives, and will likely be in the range of 10^{-3} to 10^{-6} of the yields. Values in the lower end of the range are discussed below for iodine and strontium. Cesium contents (based on high xenon releases for some mass chains) are expected to be near the upper part of the range. The effort during this quarterly period was directed toward the following specific objectives:

1. Determining the quantities of the various cesium, strontium, iodine, and tellurium isotopes found in the charcoal trap by a combination of absolute gamma spectrometry and mass spectrometric and neutron activation analyses.

2. Determining the axial dependence, if any, of the isotopic concentrations.

3. Calculation of the fractions of these isotopes found in the charcoal trap, based on the inventories generated in the fuel during the lifetime of the capsule.

4. Determination of the migrating species by analysis of the isotopic ratios for the chemical elements and comparison of the ratios with the isotopic half-lives or the half-lives of the precursors.

All of the analytical determinations of the isotopic contents of the charcoal have been completed and some of the data have been analyzed. The

analyses of the remaining data will be delayed until burnup analyses have been received from ANL and the final report on the GB-9 postirradiation examination is prepared.

The isotopic cesium analyses of the axial sample from the charcoal trap were reported in the previous quarterly report.[1] Combining the isotopic distributions with absolute gamma-spectrometry data for CS^{137}, the concentration of the cesium isotopes in the axial charcoal samples can be obtained. These are given in Table 5.1; as expected, the concentration of each isotope decreases from the inlet to the outlet of the trap. The data in Table 5.1 need to be recompiled for further analyses by combining the Cs^{133} and Cs^{134} concentrations. This is necessary because Cs^{134} has no direct fission yield and Xe^{134} is a stable isotope. Thus, Cs^{134} is not a fission product but is produced by (n, γ) reactions on Cs^{133}. The Cs^{134} in the charcoal trap was released from the fuel in the 133 mass chain. The recompiled isotopic contents are given in Table 5.2 and the concentration profiles in the trap are shown in Fig. 5.1.

The ratios of the cesium isotopes change from the inlet to the outlet of the trap as a result of isotopic decay and isotopic concentration gradients. Detailed analyses of these data and calculations of effective diffusion coefficients in the trap will be carried out during preparation of the final report on capsule GB-9 postirradiation examination.

Table 5.1

ISOTOPIC CESIUM CONTENTS OF AXIAL SECTION OF GB-9 CHARCOAL TRAP
(In parts per million)

Trap Location[a]	CS^{133}	Cs^{134}	Cs^{135}	Cs^{137}	Total Cesium
Inlet (1)	777	4.79	795	19.2	1600
Middle (3)	525	4.25	559	15.5	1110
Outlet (4)	426	352	456	15.5	895

[a]The charcoal was separated into four axial fractions, but analyses were carried out on only three of the fractions.

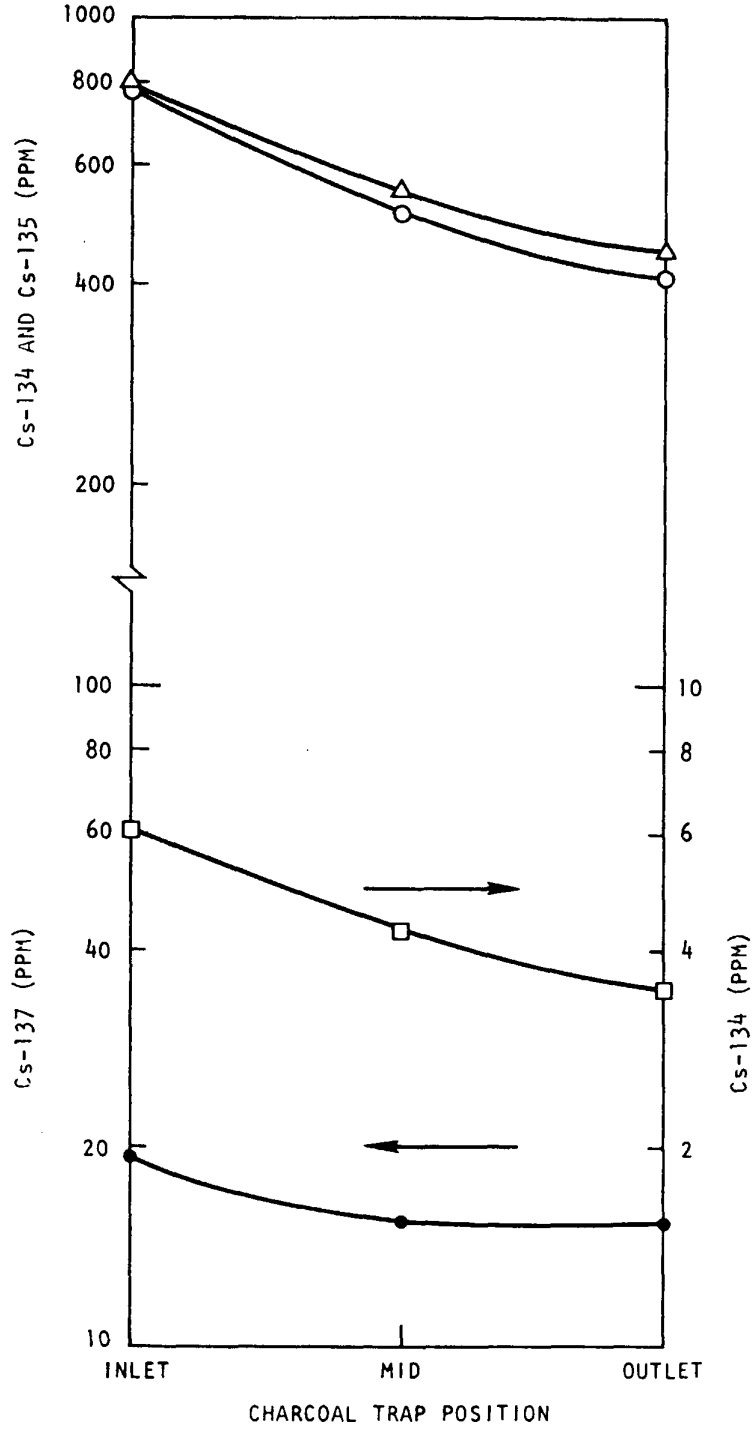

Fig. 5.1 Cesium isotopes vs. position in GB-9 charcoal trap

Table 5.2

ISOTOPIC CESIUM CONTENTS OF AXIAL SECTIONS OF THE GB-9 CHARCOAL TRAP[a]
(In parts per million)

Trap Location[b]	CS^{133}	Cs^{135}	Cs^{137}
Inlet (1)	782	795	19.2
Middle (3)	529	559	15.5
Outlet (4)	430	456	15.5

[a]Based on released mass chains.

[b]The charcoal was separated into four axial fractions but analyses were carried out on only three of the fractions.

Isotopic analyses for both I^{127} and I^{129} in three of the four axial charcoal fractions were carried out by neutron activation analyses. The results of these analyses are given in Table 5.3.

Table 5.3

ISOTOPIC IODINE CONTENTS OF AXIAL SECTIONS OF GB-9 CHARCOAL TRAP
(In parts per million)

Trap Location	I^{127}	I^{129}	Total Iodine
Inlet (1)	0.94	6.1	7.0
Middle (2)	0.87	3.6	4.5
Outlet (4)	0.37	5.2	5.6

The I^{127} yield is approximately that which would be expected from fission of U^{235} and Pu^{239} in a thermal reactor (about 20% of I^{129}). The total iodine content of the charcoal is thus in the range of 4.5 to 7 ppm, which is considerably lower than that of cesium. Iodine, however, migrates as

a volatile species and not as a fission gas since xenon is the daughter of iodine. As I^{127} is stable and I^{129} has a half-life $> 10^7$ yr, it is evident that the amounts of these isotopes measured in the trap represent the total fraction of these isotopes that migrated to the trap (since essentially none is lost by decay to the gaseous daughter followed by release) during operation of the capsule. Based on the trap charcoal loading of 1.29 g and assuming an average iodine loading of 6 ppm, the total trap assay is about 7.8 μg. Using preliminary burnup estimates based on 468 effective full-power days of operation for capsule GB-9, the iodine yields should be $I^{127} \approx 0.04$ g and $I^{129} \approx 0.15$ g for a total iodine production of 0.19 g. The fraction of total iodine found in the charcoal trap was 4.1×10^{-5}. There was no significant difference between the I^{127} and I^{129} release (as expected) on the basis of half-lives nor was there an observable axial dependence.

The charcoal was also analyzed for tellurium isotopes by activation analysis. However, the yields of Te^{126} and Te^{128} are 0.05% and 0.37%, respectively, and as the tellurium levels approached the sensitivity of the activation-analysis technique, only upper limits could be placed on the tellurium assays. Te^{128} was found to be $<<$ 40 ppm (in the inlet fraction) and Te^{126} rated from < 12 ppm to < 28 ppm.

Data on the releases of the low-mass branch species can be obtained by analyses for strontium isotopes. The migratory species are expected to be bromine and krypton, with krypton expected to be primarily responsible for the transport of the low-mass-chain nuclides. Analyses for Sr^{89} and Sr^{90} were carried out by ashing the charcoal samples, leaching the ash to extract strontium, chemical separation of the strontium, and absolute beta counting for Sr^{89} and Sr^{90}. Both isotopes were detected in each axial charcoal fraction, but the data are too scattered to determine whether or not there is an axial dependence. Using the average concentrations of Sr^{89} and Sr^{90} found in the trap and the estimated inventories based on 468 effective full power days, the fractions of Sr^{89} and Sr^{90} found in the charcoal trap were 3.6×10^{-5} and 7.2×10^{-6}, respectively.

These fractions are in the proper order based on the expected release fraction of the gaseous precursors, which are, in turn, dependent on the half-lives of the gaseous nuclides. The bromine and rubidium precursors of strontium are also a possible transporting species, as shown by the decay schemes:

$$4.4s\ Br^{89} \rightarrow 3.2m\ Kr^{89} \rightarrow 15.4m\ Rb^{89} \rightarrow 50.5d\ Sr^{89}$$

$$1.6s\ Br^{90} \rightarrow 33s\ Kr^{90} \rightarrow 2.7m\ Rb^{90} \rightarrow 28y\ Sr^{90}$$

The half-lives of both the bromine and rubidium isotopes are in the proper order to yield the observed greater release of Sr^{89}. However, both bromine isotopes have half-lives too short to be significant contributors to the migration process. The volatile rubidium precursors, however, could contribute to chain transport, although it is most likely (based on the analogy in the heavy mass chain) that the gaseous krypton nuclides are the primary contributors to the transport.

5.1.2. Irradiation Capsule GB-10

Irradiation of capsule GB-10, which was shut down on October 12, 1973, because of a leaky valve in the shielded valve box, was resumed on November 16, 1973, after the valve was replaced. The capsule was then operated at 13.5 kW/ft (630°C maximum outside cladding temperature). By January 12, 1974, a total burnup of 36,200 MWd/Te was accumulated, with 27,000 MWd/Te at 12.0 kW/ft (565°C) and 9,200 MWd/Te at 13.5 kW/ft (630°C).

The vented activity has approximately leveled out again, after an initial rise of a factor of ~6 that was followed by a more gradual rise to a total factor of ~7 times the steady level measured at 12.0 kW/ft. The steady condition now permits a number of experiments to be conducted, some of which are planned to begin in the next quarterly period, including power cycling (breathing effects), low-pressure operation (200 psi and 100 psi versus normal 1000 psi), and fission-product-mixture variations with flow rate using the Ge(Li) detector being installed on the sweep-gas sampling line (see Section 4). It is planned to complete these tests prior to raising the power to 14.8 kW/ft (685°C).

Removal of the leaky valve (noted above) and some associated tubing presented an opportunity to determine the extent and composition of fission-product deposition in the sweep-gas lines of capsule GB-10. Both the defective valve and a section of high-pressure gas-line tubing (~5 in. long) with an attached cross fitting were subjected to Cutie Pie (Nuclear Chicago Mod. 2588 ion chamber) dose rate and gamma-spectrometer measurements. The results indicate dose rates of 7 and 300 mr/hr from the valve and the tubing plus fitting, respectively. Fission and activation products I^{131}, Cs^{134}, Cs^{137}, Ba/La^{140}, and Ce^{141} were present. The Cs^{137} activity represented ~50% of the activity in the valve and 88% of the activity in the tube and fitting. The tube and fitting activity was more than 142 times that of the valve activity, compared with a dose-rate factor of ~43. (It should be noted that these gas lines are used during operation of the capsule in all flow modes.) In one flow mode—in through the bottom of the fuel and out at the interface between the top of the fuel and the bottom of the upper axial-blanket region—the capsule effluent is taken from the location where large peaks of iodine and cesium activity are found in gamma scans of both vented and sealed fast-reactor fuel rods. These data are therefore not typical of what should be expected in either nonleaking or leaking GCFR fuel rods where venting occurs from the top of the rod charcoal trap above the upper axial blanket.

Data on released and vented activity and on iodine release and transport in the GB-10 vented fuel rod taken between November 1972 and September 1973 were received from ORNL. Analyses of these data at GA will be reported on subsequently.

Work has been initiated to install continuous tritium-measuring instrumentation on the sweep-gas line of capsule GB-10. Instrumentation similar to that developed and installed at the Peach Bottom HGTR is being investigated. Since the molecular composition of tritium (i.e., HTO or HT) is not known, a section to convert HTO to HT, probably by passing the stream over hot metal, will be added. By operating with and without the converter in the line, the HT/HTO ratio will be measured since any water in the stream is trapped out before the measurement of hydrogen is made. By sweeping the fuel, axial blanket, and charcoal trap the effect of each region on the HT/HTO ratio may be measured.

The possibility of measuring the tritium released from the fuel and the fractions normally vented and permeating the 316 SS cladding at operating temperature is being investigated. The vented tritium can be measured by operating the capsule in the normal flow mode, i.e., sweeping the gases vented from the top of the fuel rod into the line leading to the measuring and sampling instrumentation. The tritium permeation of the cladding may be measured by sweeping the fueled region of the rod and measuring the tritium. Then by subtracting the vented tritium obtained in the previous measurements, the tritium permeating the wall of the 316 SS is the remainder, assuming that the sweeping gas prevents the tritium released from the fuel from entering the cladding wall and that the chemical thermodynamic conditions within the fuel rod are not significantly altered by the sweeping gas.

5.2. FAST-FLUX IRRADIATION EXPERIMENTS

5.2.1. Fast-flux Irradiation Experiment F-1 (X094B)

The irradiation of the seven-fuel-rod capsule F-1 experiment (X094B) continues in EBR-II and maximum burnup exposures up to 65,000 MWd/Te have been achieved. Irradiation of the subassembly will continue to the burnup goal of 100,000 MWd/Te on the remaining initial fuel rod (G-4); an interim examination is to be made after ~75,000 MWd/Te.

Preparations are being made at ANL to begin nondestructive and destructive postirradiation examination of the rods removed during the second interim examination in early 1973. The operating conditions for the rods are shown in Table 5.4.

One fuel rod, G-1, has been deencapsulated. Profilometry indicated an increase in diameter of ~0.001 in. (maximum). Ovality of ~0.002 in. was observed near the bottom fuel-blanket interface and a marred appearance (no diametral dimensional change) was observed near the upper fuel-blanket interface. Analysis of gamma-scanning data obtained during the second interim examination of the F-1 (X094A) subassembly continued. Axial gamma scans of the fuel and blanket regions of rods G-1, G-4, and G-8 obtained in April 1973 were analyzed to obtain an initial assessment of the fractions of volatile species iodine and cesium that migrated from the

Table 5.4

OPERATING TEST CONDITIONS

Rod Number	Peak Heat Rating (kW/ft)	Maximum Cladding Temperature (°C)	Burnup (MWd/Te)	Neutrons/cm^2 Total	E > 0.1 MeV
G-1	16.1	783	56,000	3.4×10^{22}	2.84×10^{22}
G-2	15.5	753	54,000	3.4×10^{22}	2.84×10^{22}
G-5	14.3	669	50,000	3.4×10^{22}	2.84×10^{22}
G-6	14.4	721	50,000	3.4×10^{22}	2.84×10^{22}
G-7	13.8	612	48,000	3.4×10^{22}	2.84×10^{22}

fuel to the blanket regions. During this quarter, data obtained in August 1973, shortly before reconstitution of the experiment, were also analyzed. These data included axial scans of the charcoal traps in rods G-4, G-6, and G-7. The purpose of these scans was to determine (1) which volatile species reached the charcoal trap, (2) the distribution of the volatile species in the charcoal trap, and (3) the migrating species, by data analysis if possible.

The axial gamma scans of the fuel and blanket regions have been discussed previously and plots of typical axial profiles for stable and volatile species were reported.[2] For stable (nonmigrating) species such as Zr^{95}, the axial profile showed a sharp drop in activity at the fuel-blanket interface. For volatile species such as iodine or cesium, enhanced concentrations were found at the fuel-blanket interface and some further migration into the blanket region was observed. Activity peaks of a smaller magnitude, but still indicating enhanced concentrations, were also found for the mass 140 chain. The transport of Cs^{140} over short distances was postulated to explain the observation of Ba/La^{140} concentrations.

The experimental profiles are now being analyzed to determine the fraction of each of four representative nuclides in the fuel, the blanket, and (for volatiles) the fuel-blanket interface region. The nuclides being

studied are Zr^{95}, Ba/La^{140}, Cs^{137}, and I^{131}. The observed profiles are being totaled over the entire length of the fuel, blanket, and interface regions and the fraction of the total inventory in each region is being calculated. These data are essentially complete except for an anomaly in one rod, probably due to computational difficulties. However, it appears fairly certain that two conclusions can be drawn:

1. Significant quantities of Cs^{137} and I^{131} have migrated from the fuel region to the interface region and some Cs^{137} also migrated into the blanket region.

2. Most of the inventory of these fission products (>60%) has remained in the fuel region in spite of the extensive migration.

The distribution of Cs^{134} and Cs^{137} in the charcoal traps of rod G-7 was reported previously.(1) Analyses of similar data obtained on rods G-4 and G-6 have shown essentially identical behavior, i.e., enhanced concentrations of Cs^{134} in regions where charcoal is present and lower levels where the charcoal is absent owing to the radiation-induced shrinkages observed. On the other hand, Cs^{137} showed a rather uniform distribution throughout the trap. This behavior has now been attributed to the Cs^{137} background in the air cell at the Hot Fuel Examination Facility at NRTS.

Neutron radiographs of rods G-4, G-6, and G-7 confirmed the shrinkage of the charcoal, which had been suspected on the basis of the gamma-scanning results. The neutron radiographs have now been measured to determine the fractional shrinkages in each of the compartments in each of the three rods. These data are given in Table 5.5. The shrinkage averages about 55% ± 5%. The fast fluences seen by the inlet end of the active traps in rods G-6 and G-7 are in the range of 4 to 5 x 10^{21} n/cm^2, which is approximately 2 to 2-1/2 times the expected fast fluence to the traps in the 300-MW(e) GCFR plant for 750 equivalent full-power days.

Table 5.5

VOLUME CHANGES OF CHARCOAL IN THE ACTIVE CHARCOAL TRAPS OF RODS G-4, G-6, AND G-7 IN THE F-1 EXPERIMENT AFTER 49,000 MWd/Te AS MEASURED FROM NEUTRON RADIOGRAPHS

Rod Number	Charcoal Trap Location	Identity of Section	Approximate Length (in.)	Original Length (in.)	Approximate Residual Charcoal (%)	Shrinkage (%)
G-4	Upper	1	0.20	0.5	40	60
		2	0.44	1.0	44	56
		3	0.56	1.1	51	49
		4	0.96	2.1	46	54
		5	0.88	2.0	44	56
		6	1.51	3.054	49	51
			4.55	9.754		
G-6	Upper	1	0.20	0.5	40	60
		2	0.47	1.0	47	53
		3	0.58	1.1	53	47
		4	1.02	2.1	49	51
		5	1.10	2.0	55	45
		6	1.51	3.054	50	50
			4.88	9.754		
G-6	Lower	1	0.57	1.2	48	52
		2	0.56	0.9	62	38
		3	0.50	1.3	39	61
		4	1.00	2.1	48	52
		5	1.10	2.1	52	48
		6	1.75	3.095	57	43
			5.48	10.695		

Table 5.5 (continued)

Rod Number	Charcoal Trap Location	Identity of Section	Approximate Length (in.)	Original Length (in.)	Approximate Residual Charcoal (%)	Shrinkage (%)
G-7	Upper	1	0.20	0.5	40	60
		2	0.50	1.0	50	50
		3	0.50	1.1	45	55
		4	0.87	2.1	41	59
		5	1.08	2.0	54	46
		6	1.30	3.054	43	57
			4.45	9.754		
G-7	Lower	1	0.50	1.2	42	58
		2	0.50	0.9	56	44
		3	0.51	1.3	39	61
		4	1.06	2.1	51	49
		5	1.07	2.1	51	49
		6	1.70	3.095	55	45
			5.34	10.695		

Note: No neutron radiographs were taken of the lower charcoal trap in G-4. Section 1 of the charcoal traps is towards fuel region of the rods.

5.2.2. Fast-flux Irradiation Experiment F-3

Work continued on the fabrication and assembly of the F-3 fast-flux experiment, which has been designed for irradiation in an EBR-II core position (row 4) and which will share a type J19A subassembly with an ANL Group-08 high-temperature chemistry experiment. The initial loading of the subassembly will contain ten F-3 fuel-rod capsules and nine Group-08 fuel-rod capsules. The F-3 fuel rods will achieve neutron exposures up to $\sim 1.5 \times 10^{23}$ nvt at 100,000 MWd/Te burnup. The F-3 fuel-rod cladding temperatures will range from 675°C to 750°C (maximum outside hot-spot temperature) and the linear heat-generation ratings will range from 12 to 15 kW/ft.

The assembly of 12 rods for the F-3 experiment (10 for the initial loading plus 2 spares) has been completed by ANL. The 12 rods will now be encapsulated and sodium-bonded. The fabrication of the F-3 fuel-rod capsules is now scheduled for completion by May 1974.

Some mechanically roughened cladding tubes as well as tubes roughened by etching will be employed in the fuel rods for the F-3 experiment. Those tubes roughened by Superior Tube Company were found to contain grinding scores up to 0.002 in. deep after inspection at ANL and will not be used in the experiment.

Although analysis at GA indicated that the scores, which were in the smooth section of the tubes in the blanket and plenum regions, would not compromise meeting the objectives of the experiment, DRRD placed a hold on the use of the tubes. The situation was resolved by substituting the tubes roughened by Superior Tube Company with tubes roughened by chemical etching.

Another "hold" in the assembly of one rod occurred when the stack up of pellet tolerances caused the resulting pellet stack height to be 0.032 in. longer than specified. Since the increased stack height was determined to have a trivial effect on the performance of the rod, the matter was resolved by accepting the rod fuel length "as is."

Some difficulties were experienced by ANL in welding the upper-rod xenon-tag fill-tube protection cap. The problem results from expansion due to heating of the trapped gas in the internal volume of the cap during welding, which causes "blow outs" of the cap welds; ANL is experimenting with possible remedies for this problem.

Trial fabrication samples of mockup sealed thermocouple segments to be included in the flow strips for the F-3 subassembly have been prepared and appear to be satisfactory. The samples will be sent to the EBR-II Project for evaluation.

The receipt at GA of the actual thermocouple segments is anticipated to occur late in January 1974.

REFERENCES

1. "Gas-Cooled Fast Breeder Reactor Quarterly Progress Report for the Period August 1, 1973 through October 31, 1973," USAEC, Report Gulf-GA-A12824, Gulf General Atomic, December 10, 1973.

2. "Gas-Cooled Fast Breeder Reactor Quarterly Progress Report for the Period May 1, 1973 through July 31, 1973," USAEC, Report Gulf-GA-A12728, Gulf General Atomic, October 10, 1973.

6. TASK 4700—NUCLEAR ANALYSIS AND REACTOR PHYSICS

6.1. CRITICAL EXPERIMENT PLANNING

Preanalysis has begun on typical matrix cell compositions for the GCFR critical assembly experiment. Two models have been examined. The first cell is that specified in the scoping document[1]; it utilizes a single platelet of Fe_2O_3 per repeating matrix cell. The second model utilizes two platelets of Fe_2O_3 to match the oxygen/heavy metal ratio (O/M) better. The cell nuclide densities for the two models and for the "average" GCFR core (single enrichment) are given in Table 6.1.

Utilizing the two simple simulation models, a series of homogeneous calculations employing the cross-section preparation code GGC-5[2] and the GAZE[3] and BUG-2[4] diffusion codes were performed. The first geometric size considered was the full-size core with radial and axial blanket atom densities appropriate to the ZPR simulation.[1] The second model utilized a collapsed radial blanket in which all blanket void space was replaced by U_3O_8 platelets. A comparison of the eigenvalues and spectral differences is given in Table 6.2.

Of the three cases in Table 6.2, only the last can physically be fitted or loaded in the ZPR-9 matrix. Some further study will be required to establish a single repeating matrix cell for Assembly 1. Concurrently, an examination of unit cells repeating in composition every second or third row is being undertaken. More flexibility in composition and the increased variations in enrichment possible are expected to result.

6.2 LIAISON WITH ARGONNE NATIONAL LABORATORY

The frequency of contacts with the Applied Physics Division at ANL is increasing as the joint planning for the GCFR critical experiments is expanded. A meeting was held in San Diego on February 7 and 8, 1974.

Table 6.1

MATCHED NUCLIDE DENSITIES

(atoms/cm^3 (x 10^{21}))

Nuclide	GCFR Core Average	ZPR Simulation	
		Cell 1	Cell 2
Pu^{239}	0.8246	0.8907	Same as in Cell 1, except as noted
Pu^{240}	0.3748	0.1184	
Pu^{241}	0.2099	0.0133	
Pu^{242}	0.0899	0.0018	
U^{235}	0.0113	0.0091	
U^{238}	4.4363	4.153	
Mo	0.2660	0.2391	
Fe	9.170	11.869	13.623
Ni	1.810	1.299	
Cr	2.310	2.838	
Mn	0.0	0.223	
O	11.890	7.325	10.254
Total fissile Pu	1.0344	0.904	
Total fertile (238 + 240)	4.811	4.271	
O/M ratio	2.0	1.41	1.98
Enrichment	0.177	0.175	

Table 6.2

COMPARISON OF CELL MODELS

Model	k_∞	k_{eff}		Median Flux Energy (keV)
		1D	2D	
Cell 1	1.632	0.9887	---	207.3
Cell 2	1.544	1.0080	1.0067	178.5
Cell 1 with collapsed radial blanket	1.544	0.9908	---	---

6.3. METHODS DEVELOPMENT AND COMPARISON

One difference between ANL and GA diffusion calculations is that the ANL upper energy limit is 10 MeV, whereas the GA upper energy limit is 14 MeV. It is therefore important, when comparing ANL and GA diffusion calculations, to know the effect of the 10 to 14-MeV energy range on the GA results. To determine this effect, two one-dimensional GAZE calculations were run modeling the 300-MW(e) GCFR with a two-row UO_2 radial blanket.

Both cases used eleven-group cross sections (see Table 6.3). Group 1 extended from 14 MeV to 10 MeV. Groups 2 through 11 had the standard GA ten-group lower energy boundaries. In Case 1 an eleven-group fission source extending from 14 MeV to 0.414 eV was used to simulate GA methods. Case 2 had a zero fission source in Group 1 and a renormalized fission source over Groups 2 through 11. Thus, the fission source extended from 10 MeV to 0.414 eV, simulating ANL methods. All cross sections were for an average core composition.

Table 6.3

ENERGY STRUCTURE

Group	Lethargy
1	-0.4 to 0.0
2	1.0
3	2.0
4	3.0
5	4.0
6	5.0
7	6.0
8	7.0
9	8.0
10	10.0
11	17.0

The results are given in Table 6.4. The k_{eff} went down from Case 1 to Case 2 due to the high number of neutrons per fission in Group 1. The

breeding ratio, defined as captures in U^{238} + PU^{240} divided by absorptions in Pu^{239} + Pu^{241}, increased due to the lower than average ratio of captures to fissions in Group 1. The radial leakage and mid-energy of the flux did not change significantly.

Table 6.4

RESULTS OF 1-D DIFFUSION CALCULATION

	Case 1	Case 2	Change
Upper energy limit	14 MeV	10 MeV	
k_{eff}	1.09373	1.09261	-0.00112
Breeding ratio for core plus radial blanket	1.1387	1.1402	0.0015
Radial leakage per source neutron			
Core	0.1575	0.1575	
Reactor	0.0277	0.0276	
Core zone 1 mid-energy, keV	170.65	170.55	-0.10

REFERENCES

1. Moore, R. A., "A Critical Experiment Program for the 300-MW(e) Gas-Cooled Fast Breeder Reactor - Scope and Purpose," USAEC, Report Gulf-GA-A12780, Gulf General Atomic, October 1973.

2. Mathews, D. R., et al., "GGC-5, A Computer Program for Calculating Neutron Spectra and Group Constants," USAEC, Report GA-8871, General Dynamics Corporation, General Atomic Division, September 1971.

3. Lenihan, S. R., "GAZE-2, A One-dimensional, Multigroup, Neutron Diffusion Theory Code for the IBM-7090," Report GA-3152, General Dynamics Corporation, General Atomic Division, August 1962.

4. Dorsey, J. P., et al., "BUG-2/BUGTRI, Two-dimensional Multigroup Burnup Codes for Rectangular and Hexagonal Geometry," USAEC, Report GA-8272, General Dynamics Corporation, General Atomic Division, August 1969.